

Alma Mater Studiorum Università di Bologna  
Archivio istituzionale della ricerca

Masonry columns confined with fabric reinforced cementitious matrix (FRCM) systems: A round robin test

This is the final peer-reviewed author's accepted manuscript (postprint) of the following publication:

*Published Version:*

Aiello M.A., Bencardino F., Cascardi A., D'Antino T., Fagone M., Frana I., et al. (2021). Masonry columns confined with fabric reinforced cementitious matrix (FRCM) systems: A round robin test. CONSTRUCTION AND BUILDING MATERIALS, 298, 1-31 [10.1016/j.conbuildmat.2021.123816].

*Availability:*

This version is available at: <https://hdl.handle.net/11585/860381> since: 2022-02-17

*Published:*

DOI: <http://doi.org/10.1016/j.conbuildmat.2021.123816>

*Terms of use:*

Some rights reserved. The terms and conditions for the reuse of this version of the manuscript are specified in the publishing policy. For all terms of use and more information see the publisher's website.

This item was downloaded from IRIS Università di Bologna (<https://cris.unibo.it/>).  
When citing, please refer to the published version.

(Article begins on next page)

# MASONRY COLUMNS CONFINED WITH FABRIC REINFORCED CEMENTITIOUS MATRIX SYSTEMS: A ROUND ROBIN TEST

*Aiello M.A.<sup>1\*</sup>, Bencardino F.<sup>2</sup>, Cascardi A.<sup>3</sup>, D'Antino T.<sup>4</sup>, Fagone M.<sup>5</sup>, Frana, I.<sup>10</sup>, La Mendola L.<sup>7</sup>, Lignola G.P.<sup>8</sup>, Mazzotti C.<sup>6</sup>, Micelli F.<sup>1</sup>, Minafò G.<sup>7</sup>, Napoli A.<sup>9</sup>, Ombres L.<sup>2</sup>, Oddo M.C.<sup>7</sup>, Poggi C.<sup>4</sup>, Prota A.<sup>8</sup>, Ramaglia G.<sup>8</sup>, Ranocchia G.<sup>5</sup>, Realfonzo R.<sup>9</sup>, Verre S.<sup>2</sup>*

<sup>1</sup>University of Salento, Department of Innovation Engineering, via per Monteroni, Lecce – 73100, Italy;

<sup>2</sup>University of Calabria, Department of Civil Engineering, 87036 Cosenza, Italy;

<sup>3</sup>ITC-CNR, Construction Technologies Institute - Italian National Research Council, Bari – 70124, Italy;

<sup>4</sup>Politecnico di Milano, Department of Architecture, Built Environment and Construction Engineering, P.zza L. da Vinci 32, 20133 Milan, Italy;

<sup>5</sup>University of Florence, Department of Civil and Environmental Engineering, DICEA, Via di S. Marta 3, 50139 Florence, Italy;

<sup>6</sup>University of Bologna, Department of Civil, Chemical, Environmental and Materials Engineering, DICAM, Viale Risorgimento 2, 40136 Bologna, Italy;

<sup>7</sup>University of Palermo, Engineering Department, Viale delle Scienze, 90128 Palermo, Italy;

<sup>8</sup>University of Naples “Federico II”, Department of Structures for Engineering and Architecture, via Claudio 21, 80125 Naples, Italy;

<sup>9</sup>University of Salerno, Department of Civil Engineering, Via Giovanni Paolo II, 132, 84084 Fisciano, SA, Italy;

<sup>10</sup>University of Bologna, CIRI Buildings and Construction, Via del Lazzaretto 15/5, 40131 Bologna, Italy.

\*corresponding author

## List of symbols

The symbols used within the paper are reported herein:

- $A_c$  is the net cross-sectional area of the compressed member ( $\text{mm}^2$ );
- $A_e$  is the cross-sectional area effectively confined ( $\text{mm}^2$ );
- $A_f$  is the cross-sectional area of the dry fabric ( $\text{mm}^2$ );
- $b$  and  $h$  are the short and long side dimensions of the compressed member with rectangular cross section (mm);
- $\text{CoV}$  is the coefficient of variation;
- $E_1$  is the modulus of elasticity of uncracked FRCM (MPa);
- $E_2$  is the modulus of the cracked FRCM (MPa);
- $E_f$  is the Young's modulus of the dry fabric (MPa);
- $f_{c,m}$  is the average compressive strength of the masonry and its constituents reported in Table 3 (MPa);
- $f_{c,mat}$  is the compressive strength of the FRCM-mortar (MPa);
- $f_l$  is the maximum confinement pressure (MPa);
- $f_{l,eff}$  is the effective confinement pressure (MPa);
- $F_{max}$  is the maximum recorded load during the test (N);
- $f_{c,m,exp}$  is the experimental compressive strength of the masonry column (MPa);

- 41 •  $f_{c,m,pre}$  is the predicted compressive strength of the masonry column (MPa);
- 42 •  $f_{mcd}$  is the design compressive strength of confined masonry column (MPa);
- 43 •  $f_{md}$  is the design compressive strength of unconfined masonry column (MPa);
- 44 •  $g_m$  is the mass density of the masonry ( $kg/m^3$ );
- 45 •  $k'$  is the dimensionless coefficients for strength increment;
- 46 •  $k_a$  is the shape factor;
- 47 •  $k_H$  is the dimensionless coefficient of efficiency in the horizontal direction;
- 48 •  $k_{mat}$  is the dimensionless coefficient accounting for the effect of inorganic matrix;
- 49 •  $n$  is the number of fabric layers (-);
- 50 •  $P$  is the axial load applied during the compressive test of the column (N);
- 51 •  $P_{cr}$  is the first axial cracking load of the column;
- 52 •  $r_c$  is the corner radius of the column;
- 53 •  $s$  is the maximum slip recorded during the lap shear test (mm);
- 54 •  $t_f$  is the equivalent thickness of the fabric (mm);
- 55 •  $t_{mat}$  is the total thickness of the FRCM (mm);
- 56 •  $\alpha_1$ ,  $\alpha_2$  and  $\alpha_3$  are the strength increment coefficients (-);
- 57 •  $\gamma_m$  is the partial factor for materials and products;
- 58 •  $\varepsilon_{fd}$  is the design tensile strain of the FRCM (-);
- 59 •  $\varepsilon_{fe}$  is the effective ultimate tensile strain of the FRCM (-);
- 60 •  $\varepsilon_H$  is the lateral strain of the columns (-);
- 61 •  $\varepsilon_{lim,conv}$  is the conventional strain limit defined by bond test (-);
- 62 •  $\varepsilon_u$  is the ultimate tensile strain of the FRCM (-);
- 63 •  $\varepsilon_{u,f}$  is the ultimate tensile strain of the fabric (-);
- 64 •  $\varepsilon_V$  is the vertical strain of the columns (-);
- 65 •  $\eta_a$  is the environmental conversion factor (-);
- 66 •  $\rho_{mat}$  is the matrix reinforcement ratio (-);
- 67 •  $\sigma_{lim,b}$  is the conventional stress limit of the FRCM (MPa);
- 68 •  $\sigma_{lim,conv}$  is the mean conventional stress limit (MPa);
- 69 •  $\sigma_t$  is the tensile stress in the FRCM in Fig. 7 (MPa);
- 70 •  $\sigma_u$  is the ultimate tensile stress of the FRCM (MPa);
- 71 •  $\sigma_{u,f}$  is the ultimate tensile stress of dry fabric (MPa);
- 72 •  $\sigma_V$  is the axial stress of the column (MPa);
- 73 •  $\sigma_{Vmax,RM}$  is the compressive strength of the confined masonry column (MPa);
- 74 •  $\sigma_{Vmax,URM}$  is the compressive strength of the unconfined masonry column (MPa).

## 75 Abstract

76 The conservation and the preservation of existing masonry buildings, most of them recognized as cultural  
77 heritage, require retrofitting techniques that should reduce the invasiveness and assure reversibility and  
78 compatibility with the substrate. In this perspective the strengthening system should be able to improve the  
79 bearing capacity of the structural member and, at the same time, to assure mechanical and material  
80 compatibility. The use of *Fabric Reinforced Cementitious Matrix* (FRCM) composites is now recognized to  
81 be suitable for these purposes. In fact, the inorganic matrix has comparable properties with respect to the  
82 existing historical mortars while the fabric has relevant tensile strength. At the same time these systems assure  
83 satisfactory level of reversibility (or at least removability). In this scenario, the present research aims to  
84 investigate the FRCM-confinement of masonry columns focusing on the influence of specific parameters, still  
85 poorly investigated, in order to deeply understand their effect on the mechanical response. In particular, the  
86 experimental variables are: the type of masonry substrate (*Tuff* and clay brick with lime-based mortar), the  
87 type of FRCM system (glass dry mesh + lime-based mortar and steel mesh + lime-based matrix) and the  
88 number of plies (1, 2 and 3). In addition, a detailed experimental characterization of the utilized materials has  
89 been carried out, including bond test between the reinforcement and the substrate. The results evidenced that

90 the FRCM is an effective solution for masonry column confinement once a proper design is performed, taking  
91 into account all involved parameters. The different strengthening systems exhibited different failure modes.  
92 Generally, a single ply of external reinforcement produced a negligible increase of bearing capacity. Both  
93 strengthening systems applied with multi-ply strengthening schemes produced a significant increase in terms  
94 of strength and ultimate axial deformation. This benefit was observed for both *Tuff* and clay masonry columns.

95 Two available design-oriented formulas, reported in Italian CNR (*National Research Council*) and ACI  
96 (*American Concrete Institute*) guidelines have been utilized, in order to further investigate their availability,  
97 mostly in case of multi-layered reinforcement. The performed comparisons highlight that the two design  
98 relationships provide similar and accurate results when referred to the GFRCM (*Glass-FRCM*) system in 1-  
99 and 2-layers' configurations, while the predictions appear conservative when 3 layers of GFRCM are utilized,  
100 for both masonry types. Considering the SRG (*Steel Reinforced Grout*) system the results predicted by the two  
101 models are more scattered, mostly when the number of layers increases. In addition, the formulation proposed  
102 by CNR appears more accurate in case of *Tuff* masonry while the ACI predictions are closer to the experimental  
103 results in the case of clay brick masonry.

104 **Keywords:** masonry, FRCM, confinement, design-oriented model, testing, columns.

105

## 106 **Introduction**

107 A large number of existing masonry structures requires strengthening or retrofitting solutions due to seismic  
108 events, long-term degradation, creep, foundation settlements, construction defects/manipulations, or increased  
109 capacity demand due to overloads. The use of fiber-reinforced materials, in place of traditional techniques such  
110 as steel ties or reinforced concrete jackets, has been largely investigated in the last decades [1]-[2]. Composite  
111 materials made by high-strength fiber sheets embedded within organic matrices, referred to as *Fiber-*  
112 *Reinforced Polymer* (FRP), were extensively used as *Externally Bonded Reinforcement* (EBR) of both existing  
113 masonry and concrete structures. A number of experimental and theoretical studies were published in the  
114 literature over the years, thus showing the strong interest by the scientific community and industry towards the  
115 application of these appealing materials [4]-[12]. FRPs present high strength-to-weight ratio, good durability,  
116 and possibility of being *ad hoc* engineered to meet the targeted structural requirements. However, the use of  
117 organic adhesives raised some drawbacks when applied to masonry structures. The poor composite-substrate  
118 compatibility, the low permeability of the strengthened surface, and the difficulties in removing the FRP sheets  
119 without damaging the substrate generated some limits to the applications in this field [13]-[14].

120 In an attempt to overcome these issues, the organic binder was replaced with an inorganic matrix and the high-  
121 strength fiber sheet with a high-strength open-mesh textile. In this way a new type of fiber-reinforced  
122 inorganic-matrix composite was proposed, usually referred to as *Fabric Reinforced Cementitious Matrix*  
123 (FRCM) [15]-[16] or *Textile Reinforced Mortar* (TRM) [17]. The name *Steel Reinforced Grout* (SRG) is  
124 adopted when the textile is made by steel cords [20]-[19]. As in the case of FRPs, FRCMs can be applied as  
125 EBR on masonry members and were proven to be effective in increasing both the in-plane and out-of-plane  
126 capacity of masonry walls [21]-[22], collapse loads of masonry arches [23], and compressive strength of  
127 masonry columns [24]-[30]. FRCMs can be made using different types of fiber (e.g. glass, basalt, carbon,  
128 *poliparafenilene benzobisoxazole* – PBO, hemp, flax, and steel in the case of SRG) and different matrices (e.g.  
129 lime-based, cement-based, and geopolymers), which combination leads to different physical and mechanical  
130 properties of the composite. The main advantages of FRCMs when compared with FRPs consist of high  
131 compatibility with poor substrates (i.e. ancient masonry) and satisfactory reversibility of the application. As  
132 well known, the last issue is crucial and quite controversial; finding the optimal compromise between safety  
133 and conservation is still challenging and some studies have been also focused on the assessment of reversible  
134 FRPs strengthening techniques [31].

135 Due to the different behaviors observed for FRCM composites, research studies were carried out to identify  
136 the main parameters that characterize the mechanical response of these materials. In light of available

137 researches, the first recommendations for design were published [15] and [32]. Within the framework of the  
138 Rilem Technical Committee 250-CSM (*Composites for the Sustainable strengthening of Masonry*), a *Round*  
139 *Robin Test* (RRT) focused on the tensile response and bond behavior of various FRCCMs considering different  
140 masonry substrates. The results were useful to provide indications for testing and to gain a better insight into  
141 the mechanical performances of each specific material [33]-[40].

142 Although numerous studies regarding the tensile and bond behavior of FRCCM composites can be found in the  
143 literature and *Initial Type Testing* (ITT) and design guidelines are currently available, some issues still remain  
144 unsolved. Among them, the identification of the contribution of the FRCCM-confinement of masonry columns  
145 is one of the most debated. Available research indicates that several parameters affect the contribution of the  
146 FRCCM jacket to the axial capacity of masonry columns. They include the mechanical and geometrical  
147 properties of substrate and composite, number of textile layers and matrix thickness, and textile and matrix  
148 maximum strain capacity [41]-[44]. Experimental outcomes showed that increasing the number of textile  
149 layers may increase the axial strength and deformability of the column [45]. However, this increase is affected  
150 by the type of FRCCM and by the column cross-section aspect ratio [47]. In some cases, a low number of textile  
151 layers may lead to negligible increments of the column axial strength, although the deformation capacity may  
152 increase [48]. Therefore, the number of textile layers appears one of the crucial parameters for the reliable  
153 evaluation of the strengthening effectiveness. Although analytical models were proposed to predict the  
154 behavior of FRCCM-confined masonry columns [15], [32] and [42]-[44], further investigations are needed to  
155 assess the models accuracy and reliability with respect to different parameters.

156 In this paper, the results of a RRT campaign on masonry columns made by clay bricks and *Tuff* stone, and  
157 confined with different number of layers of either glass FRCCM or SRG are presented and discussed. The RRT  
158 program was organized within the framework of the ReLUIIS-DPC 2019–2021 project (WP 14) funded by the  
159 *Italian Department of Civil Protection* and involved 8 universities. The experimental variables investigated  
160 are: the type of masonry (clay brick or *Tuff* stone), FRCCM type (glass FRCCM or SRG), and number of  
161 reinforcement layers (from 1 to 3 layers). The obtained results help to gain an insight on the contribution of  
162 the FRCCM to the axial behavior of confined masonry columns, mostly referring to the influence of the number  
163 of layers varying the type of masonry and the reinforcement. In addition, the comparison between experimental  
164 results and those predicted by using the two available guidelines, namely CNR-DT215 [32] and ACI 549-R13  
165 [15], are reported and discussed.

## 166 **Experimental program**

167 The experimental program aimed to investigate the mechanical behavior of masonry columns confined by  
168 multi-ply FRCCM systems and subjected to uniaxial compressive load. Their application, indeed, often involves  
169 the use of multiple layers in order to accomplish design requirements, due to the low fibers density generally  
170 characterizing such systems. A RRT was, thus, performed, involving eight Italian laboratories: University of  
171 Bologna (*UniBo*), University of Calabria (*UniCal*), University of Firenze (*UniFi*), Polytechnic of Milan  
172 (*PoliMi*), University of Naples – Federico II (*UniNa*), University of Salento (*UniSal*), University of Salerno  
173 (*UniSa*) and University of Palermo (*UniPa*). Two different types of masonry, commonly adopted in Italy, were  
174 used to build the columns, namely clay bricks and *Tuff* stones; in both cases a lime-based mortar was employed  
175 as binder, as traditionally made for historical masonry. Moreover, two types of FRCCM were used: glass dry  
176 mesh and steel wires sheet, both embedded in a lime-based mortar. The two systems will be referred in the  
177 following as GFRCCM (*Glass Fabric Reinforced Cementitious Mortar*) and SRG (*Steel Reinforced Grout*). For  
178 the first FRCCM system an adhesion promoter, labeled IPN (*Interpenetrated Polymer Network*), was used  
179 according to the manufacturer's instructions, in order to improve the bond between the inorganic matrix and  
180 the reinforcing fibers.

### 181 ***Test program, specimens and realization***

182 A total of 64 half-scale column specimens were built: 32 columns (24 confined and 8 unconfined) were  
183 prepared at *UniSal*, while 32 columns (28 confined and 4 unconfined) were prepared at *UniBo*. The columns

184 were strengthened by a variable number of reinforcement plies. The experimental work plan is reported in  
 185 Table 1.

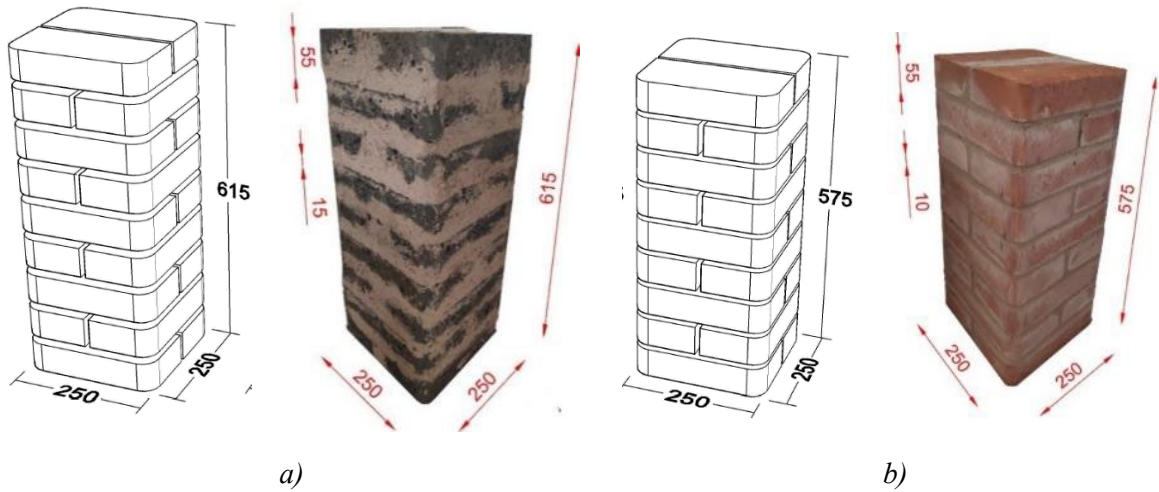
186 **Table 1. Round robin work plan.**

Construction laboratory	Testing laboratory	Masonry substrate	FRCM	# ref. column	# 1-ply column	# 2-ply column	# 3-ply column
<i>UniSal</i>	<i>UniSal</i>	<i>Tuff</i>	GFRCM	2	2	2	2
	<i>UniPa</i>			2	2	2	2
	<i>UniCal</i>	Clay brick		2	2	2	2
	<i>UniNa</i>			2	2	2	2
<i>UniBo</i>	<i>UniFi</i>	<i>Tuff</i>	SRG	1	3	2	2
	<i>UniSa</i>			1	3	2	2
	<i>UniBol</i>	Clay brick		1	3	2	2
	<i>PoliMi</i>			1	3	2	2

187

188 The geometrical dimensions of the specimens are reported in Fig. 1. The bricks had the same dimensions for  
 189 both types of masonry, i.e. 125x250x55 mm<sup>3</sup>, while the horizontal mortar joints thickness was 10 mm and 15  
 190 mm for the clay brick and the *Tuff* columns, respectively. A corner radius of 20 mm was realized along the  
 191 height of the specimens to avoid possible premature failure of the fibers, due to stress concentration at the  
 192 corners (knife-effect). The rounding of the corners was made for each block, by using a computer aided  
 193 manufacturing tool in order to minimize the possibility of manpower error.

194



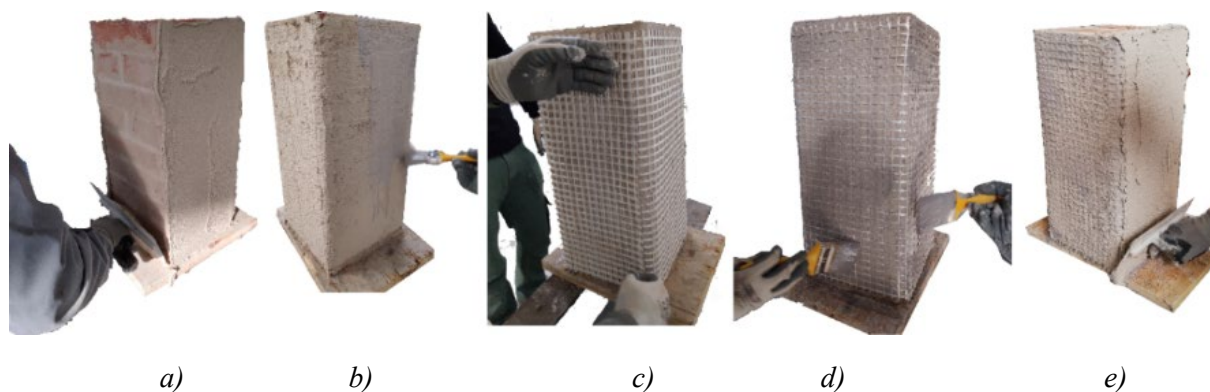
195 **Fig. 1. Specimens dimensions, in mm. a) Tuff stone and b) clay brick masonry.**

196 The confining system used at *UniSal* consisted of a lime-based mortar and a dry glass mesh; the spacing of the  
 197 mesh was 12x12 mm, with a 60 mm<sup>2</sup>/m equivalent thickness in the two orthogonal directions and a density of  
 198 300 g/m<sup>2</sup>. The reinforcement used at *UniBo* consisted of a hydraulic lime-based mortar and a sheet of  
 199 unidirectional steel wires made by high strength galvanized steel cords, with a density of 670 g/m<sup>2</sup> and cross-  
 200 sectional area of each cord equal to 0.538 mm<sup>2</sup>. The steel cords were held together by a glass fiber mesh, to  
 201 facilitate the installation of the reinforcement.

202 The FRCM installation's procedure is illustrated in Fig. 2 and Fig. 3. Preliminarily, all the columns surfaces  
 203 were soaked in order to quasi-saturate the masonry. A first layer of mortar (5 mm thick) was applied; then, the

204 specimens were wrapped by the glass grid/steel sheet with an overlapping length  $\geq \frac{1}{4}$  of the perimeter of the  
 205 cross-section; in particular an overlapping length of 375 mm and 250 mm was adopted for SRG and GFRCM  
 206 systems, respectively. The mortar was forced to go through the voids of the grid by pressing it with a trowel,  
 207 for a proper impregnation. For the single layer-reinforcement, the final step consisted in covering the grid, wet-  
 208 on-wet, with a second layer of mortar ( $\approx 5$  mm thick). For the 2<sup>nd</sup> and 3<sup>rd</sup> mesh layers, the application procedures  
 209 described above were repeated, achieving a total thickness of 15 mm and 20 mm, respectively. In the case of  
 210 multi-layers confinement, the overlapping portion for each layer was positioned on different faces of the  
 211 column, to avoid a weak region in the confinement jacket. In the case of GFRCM, the glass mesh was applied  
 212 with a single full-height grid around the column, while for SRG two sheets were utilized, each covering half  
 213 of the column's height, as prescribed by the manufacturer. In addition, the application of the GFRCM system  
 214 involved the use of an adhesion promoter, IPN-01 type basically aimed at protecting the fibers from the alkaline  
 215 environment of the mortar and at improving the bond between the mesh and the mortar. It was applied along  
 216 the lateral surfaces of the columns before and after the positioning of the glass mesh, and activated by the  
 217 humidity of the mortar. Once realized, specimens were cured for at least 28 days in laboratory conditions and  
 218 then sent to the other university partners to be tested.

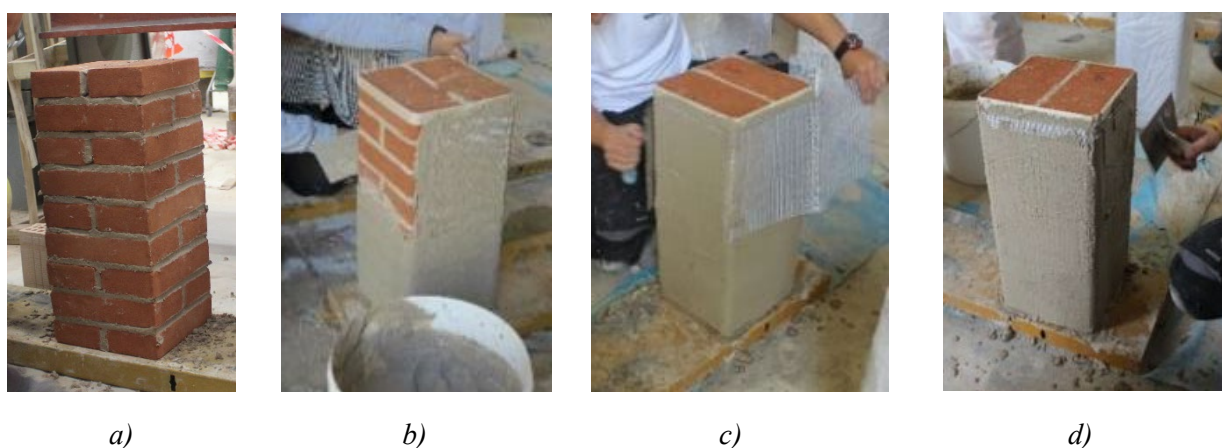
219



220

221

222 **Fig. 2. GFRCM-confinement phases: a) first mortar layer, b) first layer of IPN-01, c) glass fabric wrapping, d)**  
 223 **second layer of IPN-01 and e) second layer of mortar**



224

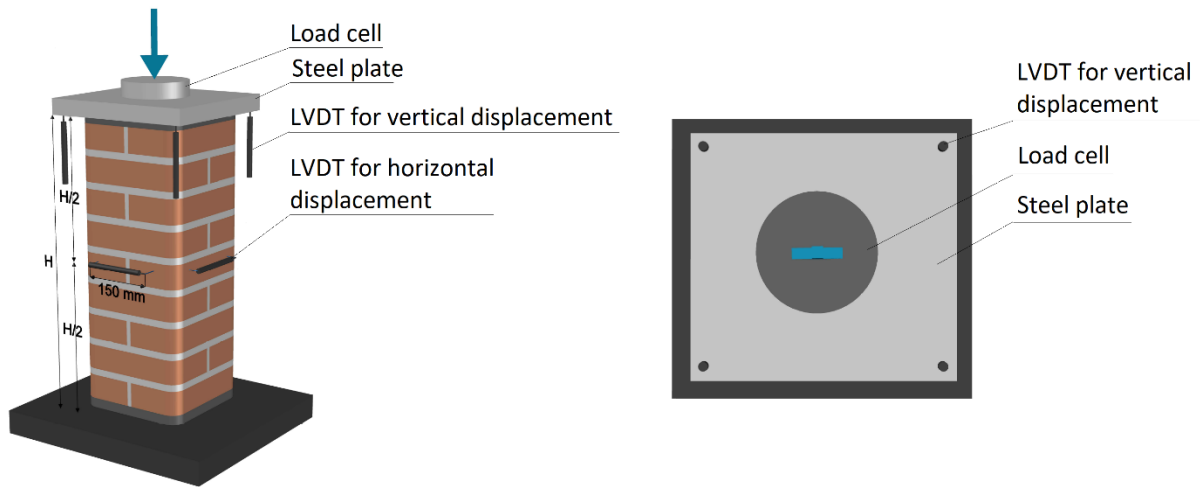
225

**Fig. 3. SRG-confinement phases: a) clay brick column, b) first layer of mortar, c) steel sheet wrapping, d) second layer of mortar.**

226  
227  
228

### Test set-up

Compressive tests were carried out in all the 8 laboratories involved in the research activity by using specifications shared between them and according to the test arrangement shown in Fig. 4.



229

230 **Fig. 4. Scheme of the test set-up.**

231 It has to be noted that, in order to prevent any contact of the FRCM jacket with the steel plate distributing the  
232 axial load on the column and, thus, the occurrence of local buckling of the jacket, a small portion at both the  
233 top and bottom of the confined specimens, approximately 10 mm high, was always left unconfined.

234 Although in the present RRT common procedures were agreed and basically respected, slight differences in  
235 the test equipment and set-ups were observed and will be discussed in the following (see also Table 2). Most  
236 labs used a hydraulic testing machines, the others a hydraulic jack or actuator; moreover, except at the UniBo,  
237 UniCal and UniSal, tests were carried out in displacement control at a rate ranging between 0.3 and 0.5  
238 mm/min, up to the failure. In order to detect the post-peak behavior, the softening phase was continued up to  
239 a conventional collapse, for tests performed in load control. The latter being generally identified on the  
240 softening branch when the measured force was about 80% of the peak load (“conventional collapse”).  
241 Horizontal elongation and vertical shortening as well as the axial load were recorded. To measure the formers,  
242 most of the laboratories used *Linear Variable Displacement Transducers* (LVDTs), directly connected to the  
243 FRCM specimens; in some cases, potentiometers were also used. In particular, four measures were recorded  
244 by each lab for both axial shortening and transverse elongation; vertical transducers were often placed at the  
245 corners of the specimens, thus allowing for both the measurement of the axial shortenings and the verification  
246 of possible load eccentricities during the test. The data acquisition frequency was not the same for all the  
247 laboratories but a minimum of 2 Hz was always assured in order to register a sufficient amount of readings.  
248 Test results are mainly given in terms of maximum and ultimate load and corresponding vertical and lateral  
249 deformations; therefore, the corresponding axial stress-axial strain curves and axial stress-lateral strain  
250 responses were obtained and plotted for each tested specimen. Fig. 5 shows some pictures of the various test  
251 set-ups.

252 Some specific remarks characterizing the experimental program should be taken into consideration; they are  
253 listed in the following:

254

- 255 • in some labs, the unconfined masonry specimens were weighted before testing in order to obtain the  
256 actual mass density; *Tuff* and brick-based masonry specimens were characterized by a mass density  
257 equal to about  $14 \text{ kg/m}^3$  and  $16 \text{ kg/m}^3$ , respectively.



- 258
- 259
- 260
- 261
- 262
- 263
- 264
- 265
- 266
- When the end surfaces were not perfectly parallel, a capping with a layer of high-strength mortar or similar material was applied at both the bottom and the top of the columns (this is the case of the Universities of Bologna, Naples and Palermo for confined columns) or only at the top (this is the case of the University of Florence and Palermo for all the specimens and just for the unconfined columns, respectively) as shown in Fig. 6.
  - In some cases, low-level load cycles were performed before starting the test in order to check the experimental set-up. In particular, the Universities of Bologna, Naples, Palermo and the Polytechnic of Milan performed cycles between 40 and 50 kN before starting with the monotonic increase of the axial displacement up to collapse.

267 **Table 2. Description of the test set-up per laboratory.**

Lab	Testing machine	Measuring tools for Load	Measuring tools for Axial Displacements	Measuring tools for Horizontal Displacements	Test performed in	Rate
<b>UniBo</b>	Hydraulic universal testing machine (60 kN capacity)	Pressure transducer (5 bar)	4 LVDTs with a recording length of 50 mm	4 LVDTs with a recording length of 20 mm applied at mid-height (gauge length 150mm)	Load control	4 N/s
<b>UniCal</b>	Hydraulic jack	External load cell of (10 KN)	4 LVDTs	4 LVDTs with a gauge length equal to 150 mm	Load control	40 N/s
<b>UniFi</b>	Hydraulic press (3 tons full-scale)	Resistance load cell (2 tons full-scale)	4 resistance displacement transducers (full-scale 1mm)	4 P-shape resistance displacement transducers (full-scale $\pm 5$ mm, allowed gauge length from 1 to 150 mm, used gauge length 150 mm)	Displacement control	0.4 mm/min (up to the conventional ultimate load) 1 mm/min from such ultimate load to the end of test
<b>UniSal</b>	Hydraulic Jack	External load cell (30 tons)	4 LVDTs with a gauge length of 1 mm	4 LVDTs applied at mid-height (gauge length 150mm)	Load control	Not controlled
<b>PoliMi</b>	Servo-hydraulic universal testing machine with 25 kN capacity	25 kN load cell	4 LVDTs	4 LVDTs with a gauge length of approximately 2 mm	Displacement control	0.2 mm/min
<b>UniNa</b>	Hydraulic actuator with load capacity of 25 kN in tension and 30 kN in compressive	External 10 kN load cell	4 LVDTs	4 LVDTs with a gauge length of 150 mm placed in the midpoint	Displacement control	0.4 mm/min
<b>UniPa</b>	Universal testing machine with load bearing capacity equal to 40 kN	Pressure transducer integrated in the testing machine, according to a prior calibration with external load cell	4 Linear Variable Displacement Transducers (LVDTs)	4 LVDTs having a gauge length of 150 mm	Displacement control	0.3 mm/min
<b>UniSa</b>	Hydraulic actuator with load capacity of 30 kN in compressive and 25 kN in tension	Load cell integrated in the testing machine	4 Potentiometers (gauge length 3 mm)	4 Potentiometers applied at mid-height (gauge length 150 mm)	Displacement control	0.3 mm/min



a)



b)



c)



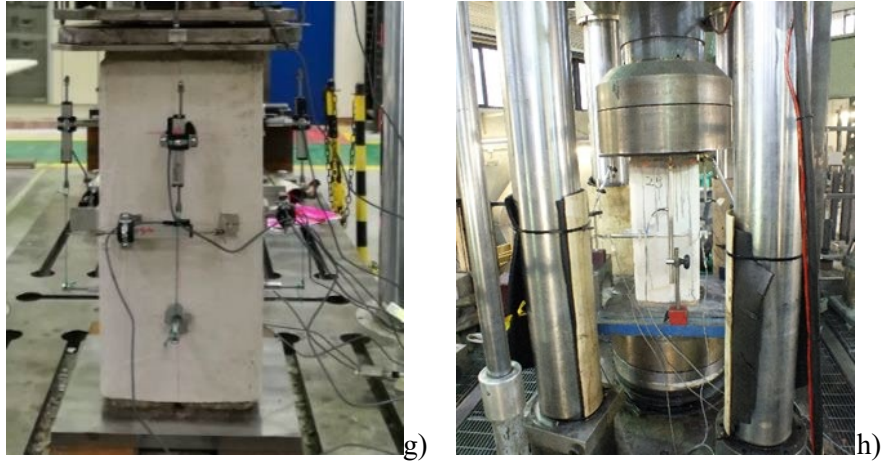
d)



e)



f)



269 **Fig. 5. Test setup - a) UniSal; b) UniBo; c) UniFi; d) UniCal; e) UniNa; f) UniPa; g) UniSa; h) PoliMi.**



270  
271 **Fig. 6. Mortar layers placed on top and bottom face of masonry specimens (UniNa).**

272 ***Materials and Bond properties***

273 The present section describes the tests realized for the mechanical characterization of all utilized materials.  
 274 Half of the characterization was carried out by *UniSal* and the other half by *UniBo*. The mortar used in masonry  
 275 joints was tested according to EN standard [49], while the compressive strength of bricks was obtained  
 276 according to [50]. In particular, a number of 30 specimens was tested for mortar. Ten cylindrical samples with  
 277 equal height and diameter (50 mm for clay bricks and 105 mm for *Tuff*) were tested for bricks. The  
 278 experimental investigation also included uniaxial compressive tests on three stacked bricks masonry prisms  
 279 [51]. The average compressive strength,  $f_{c,m}$ , for all the tested materials are reported in Table 3.

280 **Table 3. Compressive tests results**

Material	$f_{c,m}$ ( <i>UniSal</i> ) (MPa)	$f_{c,m}$ ( <i>UniBo</i> ) (MPa)
Mortar (masonry joints)	4.35 (Co.V.=0.05)	5.71 (Co.V.=0.06)
Clay brick	24.06 (Co.V.=0.14)	19.33 (Co.V.=0.08)
<i>Tuff</i> stone	5.26 (Co.V.=0.34)	5.67 (Co.V.=0.28)
Clay brick masonry prism	5.16 (Co.V.=0.15)	6.21 (Co.V.=0.07)
<i>Tuff</i> masonry prism	2.17 (Co.V.=0.20)	3.19 (Co.V.=0.10)

281

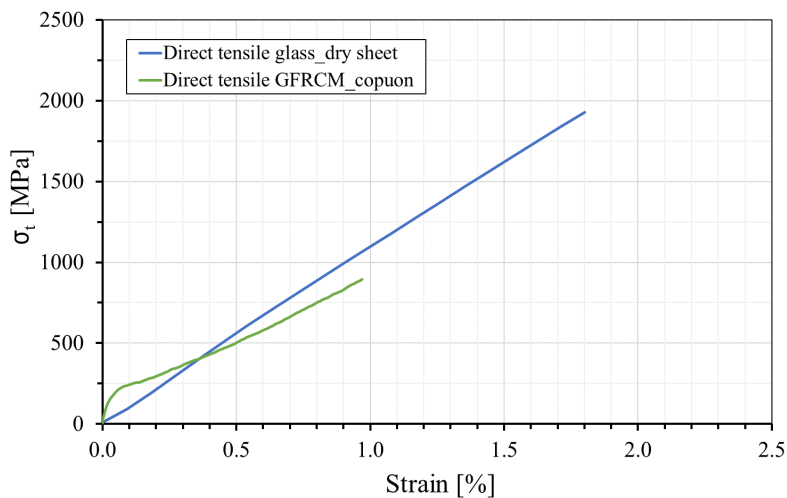
282 Regarding the GFRCM and SRG reinforcement, several specimens were prepared and tested under direct  
 283 tensile conditions, according to [52]. A total of nine GFRCM specimens were tested, sized 6x60x10 mm<sup>3</sup> and  
 284 including four longitudinal yarns of fabric spaced 12 mm (with an adhesion promoter IPN-01 type at  
 285 fabric/mortar interface); twenty SRG specimens were also tested, sized 4x40x10mm<sup>3</sup>, including five  
 286 longitudinal steel cords spaced 6.35 mm. The tensile strength, the elastic modulus and the maximum elongation  
 287 obtained from tests are reported in Table 4. For FRCM coupons, the reported elastic moduli  $E_1$  and  $E_2$   
 288 correspond to the slope of the first and of the second branch of the stress-strain curve, respectively. The tensile  
 289 strength was computed as the ratio between the peak load and the cross-section of the dry fabric.

290 The average tensile stress-strain curves of the composites systems (GFRCM and SRG) are reported in Fig. 7,  
 291 overlapped with the stress-strain curves of the corresponding dry fabric/sheet. Fig. 7a refers to GFRCMs,  
 292 where the constitutive law is characterized by a bi-linear curve with a transition curve in between. The ultimate  
 293 slope is slightly lower when compared to that of the dry fabric, while a significant reduction of the maximum  
 294 deformation and strength was registered. This result is caused by the uneven stress distribution within the fibers  
 295 after the matrix cracking that involved a premature failure of the most loaded yarns. Fig. 7b shows the stress-  
 296 strain curve for the SRG-system. In this case, the composite exhibited an almost tri-linear behavior with a third  
 297 branch more predominant with respect to the other two. The ultimate strength of the dry steel fabric was  
 298 comparable to that of the SRG; also, the scatter between the elastic modulus of the fabric and the slope of the  
 299 third branch of the stress-strain curve of SRG specimens appears negligible, while the ultimate deformation of  
 300 the SRG is slightly lower if compared with that of the dry fabric.

301 **Table 4. Tensile test results.**

Component tested	$\sigma_{u,f}$ (MPa)	$\sigma_u$ (MPa)	$E_1$ (GPa)	$E_f$ (GPa)	$E_2$ (GPa)	$\epsilon_{u,f}$ (%)	$\epsilon_u$ (%)
Glass mesh	1929 (CoV=0.14)	-	-	108.0 (CoV=0.16)	-	1.80 (CoV=0.12)	-
GFRCM coupons	-	891 (CoV=0.15)	514.5 (CoV=0.08)	-	77.5 (CoV=0.05)	-	0.97 (CoV=0.19)
Steel sheet	3080 (CoV=0.04)	-	-	193.4 (CoV=0.10)	-	2.17 (CoV=0.11)	-
SRG coupons	-	2972 (CoV=0.03)	1243.6 (CoV=0.13)	-	197.4 (CoV=0.10)	-	1.86 (CoV=0.12)

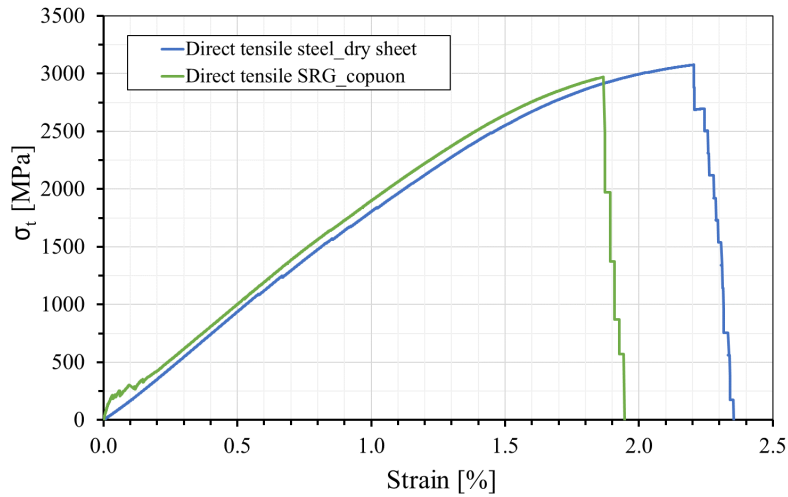
302



303

304

a)



305

306

b)

307

308

**Fig. 7. Comparison between the tensile behavior of the dry fabric and that of the inorganic based composite: a) GFRCM and b) SRG.**

309

310

311

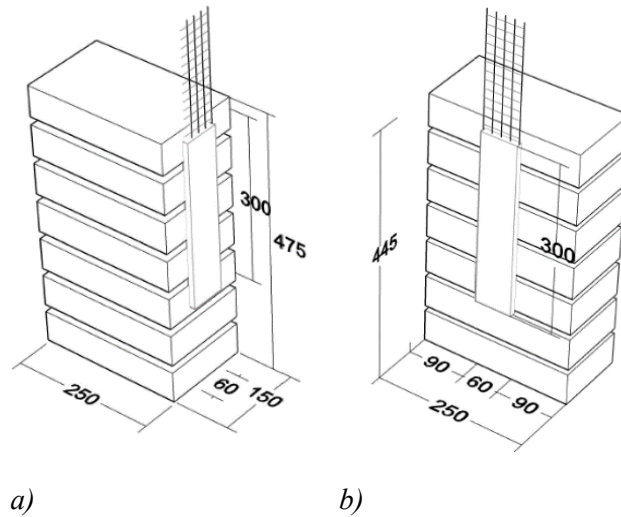
312

313

314

315

The matrix (mortars) of the two composite typologies were tested after 28 days curing to evaluate their compressive strength, according to [49]; it resulted equal to 9.1 MPa (CoV=0.27) for GFRCM, and 13.4 MPa (CoV=0.09) for SRG. Single lap shear tests were also performed in a recognized set-up, described in [35]-[39], by using the two considered masonry substrates: clay bricks and *Tuff* stones. Specimens dimensions are represented in Fig. 8; the composite strip was applied to the long faces of the clay bricks and to the short faces of the *Tuff* stones, as indicated in [53] and shown in Fig. 8. Tests were carried out under displacement control with a load rate of 0.2 mm/min. A total of 10 specimens were tested per each substrate.



a)

b)

316

**Fig. 8. Bond test specimens: a) *Tuff* substrate, b) clay bricks substrate.**

317

318

319

320

321

In Table 5 the values of the limit bond stress,  $\sigma_{lim,b}$ , the conventional limit stress,  $\sigma_{lim,conv}$ , assumed equal to the mean value of the  $\sigma_{lim,b}$  the corresponding deformation,  $\varepsilon_{lim,conv}$  and the ratio between  $\sigma_{lim,conv}$  and  $\sigma_{u,f}$  are reported. According to the CNR DT 215 [32], the limit bond stress is evaluated dividing the maximum bond load ( $F_{max}$ ) by the cross-section of the dry fabric ( $A_f$ ), while the conventional limit deformation is obtained dividing  $\sigma_{lim,conv}$  by  $E_f$ , namely the mean value of the *Young's modulus* of the fabric.

322 **Table 5. Single lap shear test results.**

<i>Lab</i>	<i>FRCM type</i>	<i>Substrate</i>	<i>Failure mode*</i>	<i>F<sub>max</sub></i>	<i>s</i>	<i>σ<sub>lim,b</sub> (F<sub>max</sub>/A<sub>f</sub>)</i>	<i>ε<sub>lim,conv</sub></i>	<i>σ<sub>lim,conv</sub>/σ<sub>u,f</sub></i>
				(kN)	(mm)	(MPa)	(%)	(%)
<i>UniSal</i>	<i>GFRCM</i>	<i>Tuff</i>	D	1.96	3.97	889.35	0.74	42
			D	2.21	3.76	16.77		
			E - F	0.97	6.52	439.89		
			E	1.89	1.48	859.39		
			E	1.96	0.86	890.10		
			B + E + A	2.09	0.54	949.29		
			E	1.54	0.83	699.84		
			B + E + A	1.51	0.52	685.21		
			<b>(Av.)</b>	1.77	2.31	802.48		
		<b>CoV</b>	23%	95%	23%			
		<i>Clay</i>	E	1.72	1.33	781.90	0.78	44
			B + E + A	1.71	1.20	778.37		
			D	1.96	3.97	889.35		
			B + E	2.03	4.18	923.29		
			B + E	2.04	8.49	929.02		
E	2.		0.44	910.39				
D	1.68		0.90	765.79				
E + F	1.79		7.16	813.76				
D	1.53		1.21	694.24				
D	2.		2.36	906.85				
<b>(Av.)</b>	1.85	3.12	839.30					
<b>CoV</b>	10%	89%	10%					
<i>UniBo</i>	<i>SRG</i>	<i>Tuff</i>	B	8.17	2.86	1899.03	0.78	49
			B	7.03	1.76	1632.88		
			B	6.03	1.78	14.02		
			B	6.51	2.34	1511.93		
			B	4.76	1.87	1105.95		
			<b>(Av.)</b>	6.50	2.12	1509.96		
		<b>CoV</b>	19%	22%	19%			
		<i>Clay</i>	B	4.94	1.25	1148.2	0.60	38
			B	4.69	1.25	1090.4		
			B	4.31	1.41	10.6		
			B	6.43	1.86	1494.2		
			B	4.77	1.49	1109.3		
			<b>(Av.)</b>	5.03	1.45	1168.55		
		<b>CoV</b>	16%	17%	16%			

323 \*according to [32]:

- 324 • A is the debonding at the matrix-substrate interface  
 325 • B is the debonding at the textile-to-matrix interface;

- 326 • D is the tensile rupture of the textile (out of the bonded area);
- 327 • E is the textile slippage within the matrix with cracking of the outer layer of mortar;
- 328 • F is the textile slippage within the mortar matrix.

329 The failure modes for the GFRCM specimens occurred at the reinforcement to-substrate interface (type A),  
330 between the textile and the matrix (type B), or by textile slippage within the matrix (type E and F). Relevant  
331 was also the case of fabric rupture (type D) which involved part of the fibers cross-section. The failure often  
332 was accompanied by micro-cracks within the matrix, at the interface between the fiber and the matrix or the  
333 matrix and the substrate. Finally, the rupture of the fabric in the free zone was also observed. For the SRG  
334 specimens, the failure occurred due to the debonding at the textile-to-matrix interface (type B) in all cases.

335 For GFRCM, obtained  $\sigma_{lim,conv}/\sigma_u$  revealed that the tensile strength of the composite system was almost  
336 reached in all the tests, independently on the failure mode and on the type of substrate. On the other hand, for  
337 SRG the conventional limit strength was significantly lower than the ultimate tensile strength of the composite  
338 system, due to the premature bond failures.

## 339 **Experimental results**

340 Experimental results achieved from monotonic compressive tests were post-processed considering the same  
341 assumptions for all the samples. In particular, the performances achieved on Un-Reinforced Masonry (URM)  
342 specimens will be used by considering that the columns were manufactured by different research units.  
343 Namely, URM columns and specimens strengthened with SRG (clay and *Tuff* masonry), were assembled at  
344 UniBo, while those strengthened with GFRCM (clay and *Tuff* masonry) were assembled at UniSal. Raw  
345 materials were provided by the same suppliers.

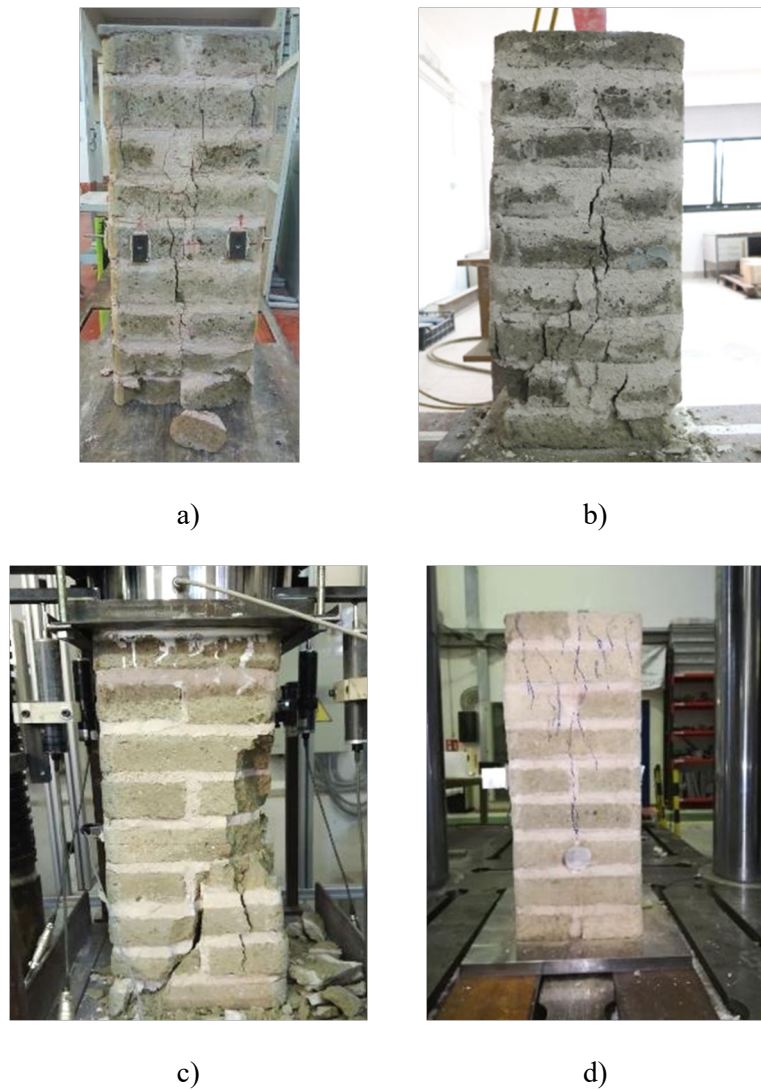
346 The assumptions made to elaborate the key experimental results were as follow:

- 347 • the axial shortening was calculated as the average of the four vertical LVDT readings (Fig. 4). The  
348 axial strain was evaluated dividing the axial displacements by the gauge length of the LVDT devices;
- 349 • the axial load  $P$ , acquired by the load cell transducer (Fig. 4), and the nominal sizes of the masonry  
350 cross-section ( $250 \times 250 \text{ mm}^2$ ) were used to evaluate the axial stress,  $\sigma_l$ ;
- 351 • the axial stress-longitudinal strain curves were stopped according to a capacity reduction in the  
352 softening phase of about 20%; for the case of hardening behavior, the ultimate value of axial strain  
353 was considered in correspondence of the maximum stress;
- 354 • the elastic modulus was calculated by evaluating the slope of the axial stress-longitudinal strain curve  
355 from the 5% to 40% of the maximum axial stress,  $\sigma_l$ ;
- 356 • the first axial cracking load,  $P_{cr}$  was assessed in correspondence of the first crack directly detected on  
357 the lateral surface of the specimen or by the discontinuity detected on the load vs displacement curves,  
358 at the end of the first almost linear branch. The second approach resulted more reliable for confined  
359 columns where the external masonry surfaces were totally covered;
- 360 • the hoop elongation/strains were evaluated by considering the average measure obtained from the four  
361 horizontal LVDT devices. The lateral measurements provided reliable results from null axial stress up  
362 to the first axial cracking load. The hoop strains measured after the formation of the first crack were  
363 often jeopardized by the detachment of the LVDT devices, due to cracking of the matrix;
- 364 • the increase in load carrying capacity was calculated as the ratio between the maximum stresses  
365 recorded for the confined specimens and that for the URM specimens. The latter being the average  
366 strength evaluated for unconfined columns made by the same manufacturer; thus, two average values  
367 were determined for each kind of masonry (referring to columns realized at UniSal and UniBo). This  
368 was considered the most rational choice in order to exclude from the elaboration stage the possible  
369 variability typically related to the hand manufacturing process, as better reported in the following. In  
370 this context, it should be mentioned that UniBo built two URM specimens for each masonry type (clay  
371 brick and *Tuff*), while UniSal built four URM columns for each masonry type.

372  
373  
374

### ***Unreinforced Tuff masonry***

Fig. 9 a-d shows representative cracks and damage patterns for URM specimens tested in the different laboratories.



375 ***Fig. 9. Unreinforced Tuff masonry specimens after testing: a) 1\_URM UniPa; b) 2\_URM UniSal; c) 1\_URM UniFi;***  
376 ***d) 1\_URM UniSa.***

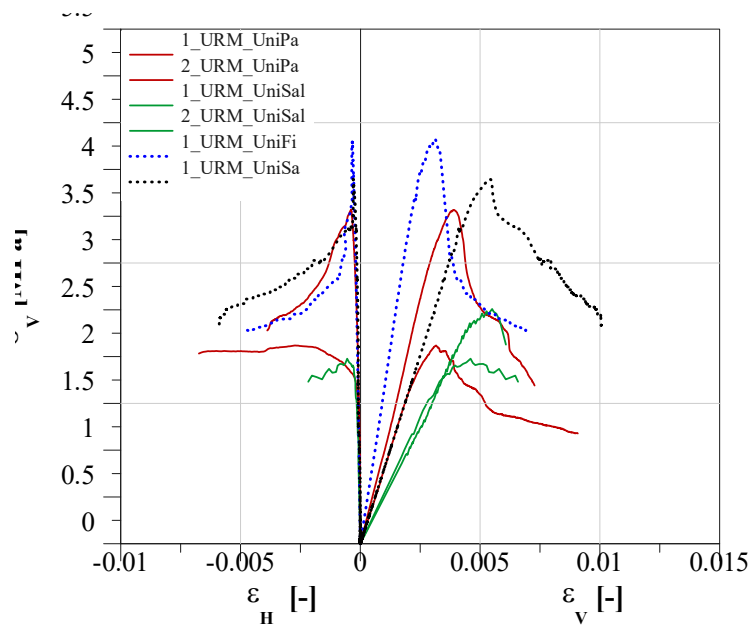
377 The failure modes were always brittle and almost similar in all cases, with several vertical cracks starting from  
378 the *Tuff* units and developing also within the mortar joints. Cracks intensified along the middle part of the  
379 specimens up to the compressive crushing of the brick units occurred; in some cases, a significant damage was  
380 recorded also near the bottom base (Fig. 9a, b, c).

381 The compressive behavior of URM columns proved to be characterized by a load carrying capacity with high  
382 dispersion and a limited softening post-peak response (Fig. 10). However, the average values resulted  
383 compatible with the compressive strength of typical *Tuff* masonries and the expected variability caused by that  
384 of constituent materials (see Table 3) and by the different hand manufacturing. Fig. 10 shows the compressive  
385 axial stress as a function of the vertical and hoop strains for all the *Tuff* URM samples experimentally tested.  
386 Curves are differently colored on the basis of the laboratory which performed the tests, while the solid or dotted  
387 line refers to the different sets of samples, selected on the basis of the manufacturing place: UniPa and UniSal



388 belongs to the same set, being manufactured by UniSal, while UniFi and UniSa belongs to another set  
389 manufactured by UniBo.

390



391

392 **Fig. 10. Axial stress vs. axial and hoop strain for unreinforced Tuff masonry specimens.**

393 The trend of the curves reflects the observed evolution of cracks and damage of the URM specimens. The  
394 initial linear trend is followed by a limited non-linear ascending branch after first cracking and up to the soon-  
395 reached peak load. The softening post peak phase is characterized by an initial almost-linear branch followed  
396 by a curvilinear behavior, corresponding to the extensive cracking stage of the specimen. The mean  
397 compressive strength of specimens tested by UniPa and UniSal was equal to 2.54 MPa and the corresponding  
398 axial strain was equal to 0.43, while the conventional ultimate strain resulted 0.55. It is worth noting that the  
399 URM samples tested by UniFi and UniSa showed a greater average compressive strength (4.11 MPa), but with  
400 values of strain at peak and of ultimate strain similar to those evaluated by UniPa and UniSal.

401 Significant scatters were observed for the measured compressive strengths, being the latter between 1.98 MPa  
402 and 3.57 MPa for specimens built in Lecce and tested by UniPa and UniSal, while it was in the range between  
403 3.89 and 4.33 MPa for columns tested by UniFi and UniSa. Differences were obtained also on the measured  
404 value of the elastic modulus in compression. The elastic modulus obtained from the tests performed by UniPa  
405 was 70% greater than that measured by UniSal; similarly, UniFi obtained a modulus equal to about twice that  
406 recorded at UniSa. These differences can be ascribed partially to the different test set-up and partially to the  
407 before mentioned variability of the masonry material.

408 It is also worth noting that the trend of the hoop strains allowed detecting the first cracking load, as the load  
409 value for which the hoop strains curves changed the slope suddenly. The corresponding force values were  
410 approximately 60% and 80% of the corresponding peak loads, respectively for specimens tested by UniPa and  
411 UniSal and by UniFi and UniSa. The experimental results are shown in Table 6, referring to the single specimen  
412 and the average values (Av.).

413

414 *Table 6. Experimental results for unreinforced Tuff masonry.*

Outputs	UniPa		UniSal		UniFi	UniSa
	1_URM	2_URM	1_URM	2_URM	1_URM	1_URM
Maximum stress [MPa]	2.12	3.57	2.51	1.98	4.33	3.89
(Av.)	(2.54)				(4.11)	
Maximum axial strain [-]	0.32	0.39	0.55	0.46	0.31	0.54
(Av.)	(0.43)				(0.43)	
Ultimate stress [MPa]	1.68	2.87	2.13	1.73	3.42	3.11
(Av.)	(2.10)				(3.27)	
Ultimate axial strain [-]	0.46	0.45	0.61	0.66	0.36	0.37
(Av.)	(0.55)				(0.37)	
Maximum hoop strain [-]	0.27	0.04	-	0.05	0.03	0.13
(Av.)	(0.12)				(0.08)	
First cracking stress [MPa]	1.44	2.40	1.23	1.17	3.69	3.18
(Av.)	(1.56)				(3.44)	
Elastic modulus [MPa]	798	987	493	540	1658	805
(Av.)	(705)				(1232)	

415 *Tuff masonry confined by Glass Textile Reinforced Mortar (GFRCM)*

416 Fig. 11 shows some representative specimens confined by the GFRCM system after the tests.

417

*Specimens tested by UniPa      Specimens tested by UniSal*

*One layer  
GFRCM*



Two layers  
GFRCM



Three layers  
GFRCM



418 **Fig. 11. Failure mode of Tuff masonry specimens confined by GFRCM.**

419 The observed failure mode was similar for all the specimens, with the formation of one main critical crack in  
420 correspondence of the edge at one corner of the column, starting from the bottom base and developing along  
421 the loading direction. This failure mode indicates, as expected, that the stress concentration at the corners,  
422 anticipates the tensile failure elsewhere, in the fibres. The tensile breakage of the glass fiber yarns was visible  
423 inside the crack, more clearly detectable for specimens confined with one layer of textile; in some cases, the  
424 slippage of the fiber from the matrix was also identified by observing a small portion of fiber filaments inside  
425 the crack. As expected, the opening of the critical crack was smaller for specimens confined with more layers  
426 and larger for one-layer confined specimens.

427 Tests highlighted the higher confinement efficiency of the multi-ply configuration schemes, as expected. Fig.  
428 12 shows the trend of the compressive strength recorded during the test ( $\sigma_{V_{max, RM}}$ ) together with its increase  
429 (dimensionless load carrying capacity), being the latter evaluated as the ratio between  $\sigma_{V_{max, RM}}$  and the average  
430 maximum stress for the URM specimens tested by UniPa and UniSal ( $\sigma_{V_{max, URM}}$ ). The experimental trend  
431 proved to be similar for the two series of samples and independent from the testing laboratory, highlighting  
432 the reliability and the repeatability of the tests. In particular, the average maximum stress of the specimens  
433 reinforced with one layer of GFRCM proved to be almost similar to the axial capacity of URM samples,  
434 meaning that the strength increase due to one-layer of glass FRCM was almost negligible; this is mainly due  
435 to the low density of fibrous reinforcement typically used in FRCM systems in relation to the significant lateral  
436 expansion of the substrate. Substantial increase of the axial capacity was observed for specimens wrapped with  
437 two and three layers. The average strength increase recorded by UniPa and UniSal were equal to 23% and 45%  
438 for two layers and 70% and 83% for three layers, respectively.

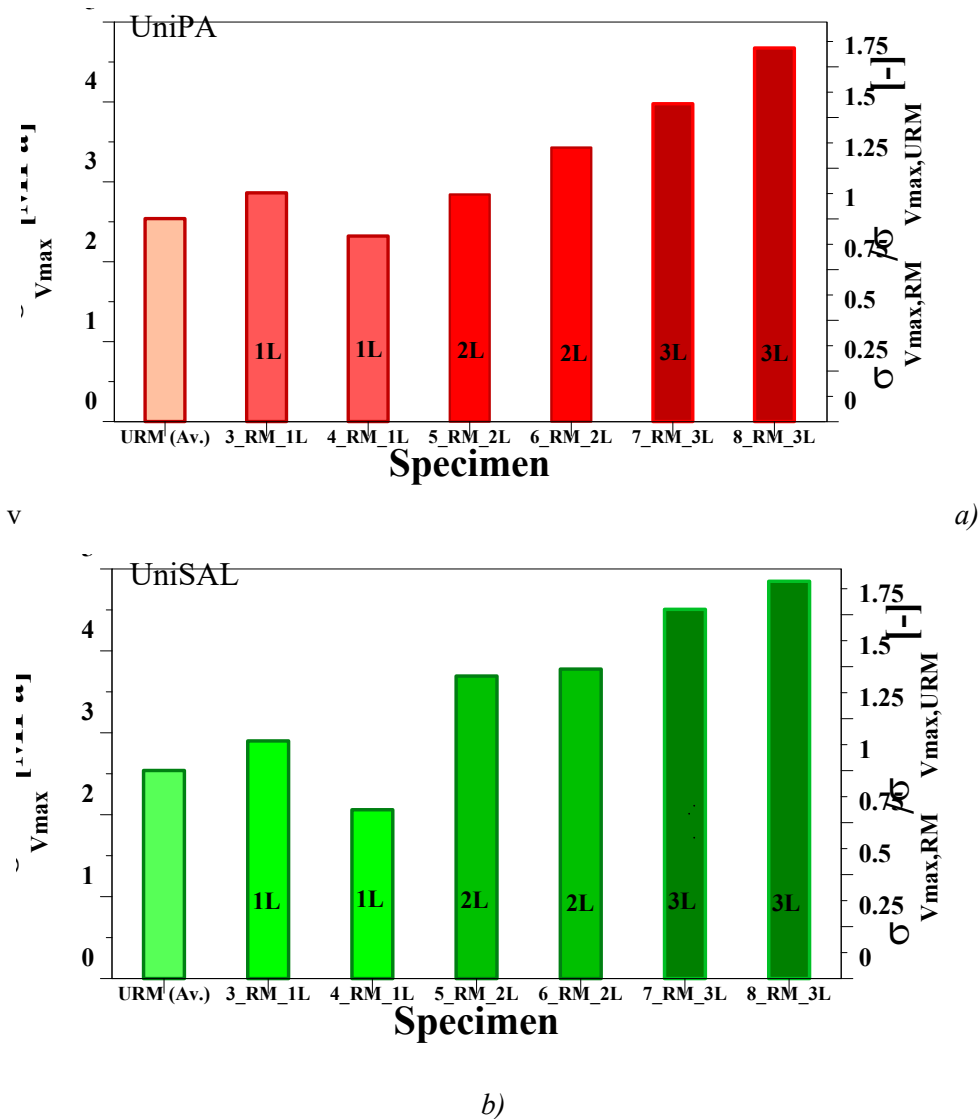


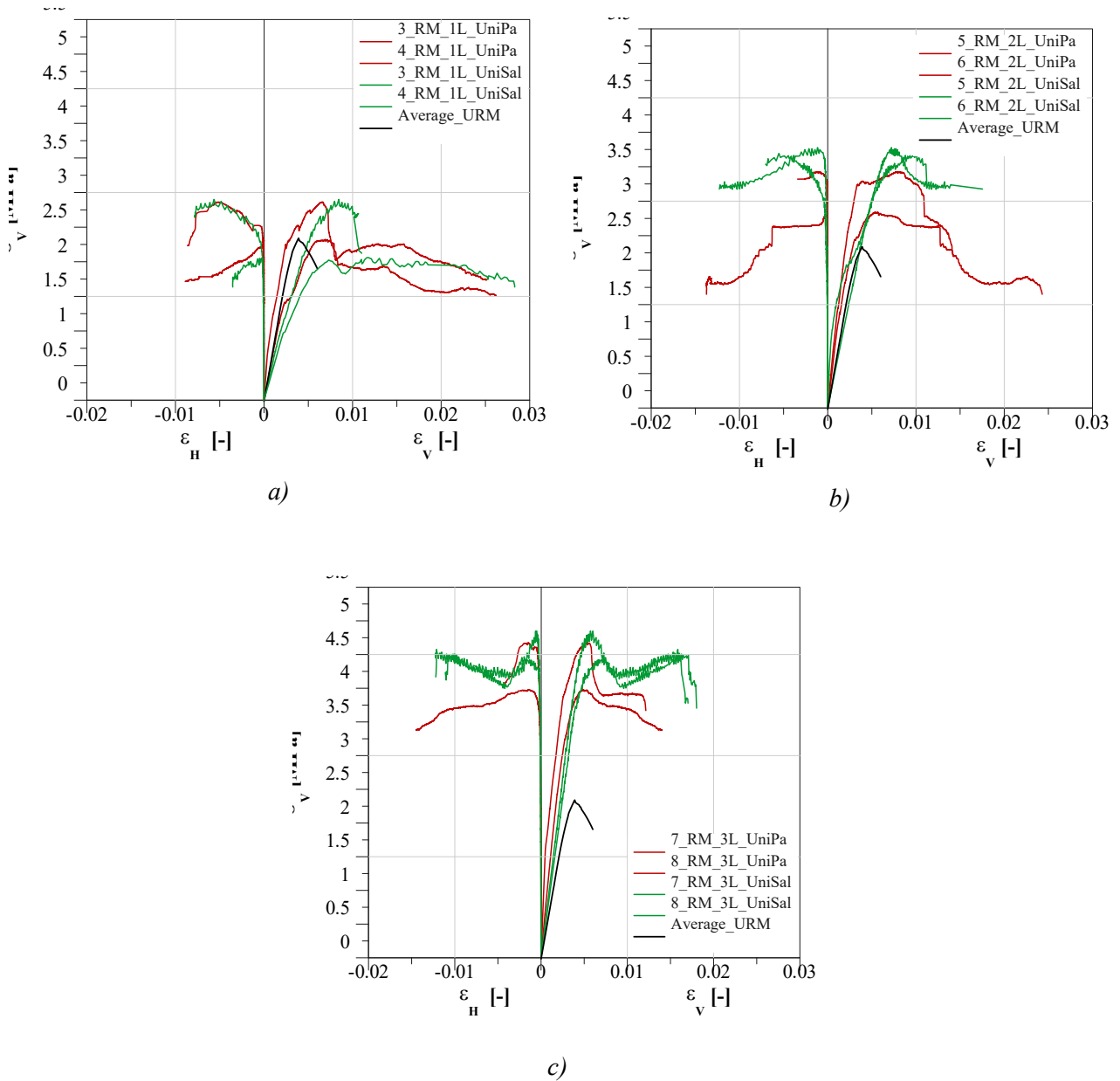
**Fig. 12. Maximum stress and dimensionless load carrying capacity of Tuff masonry columns confined by GFRCM: a) specimens tested by UniPa; b) Specimens tested by UniSal**

439 The axial stress vs axial and hoop strains (compressive behavior) of the *Tuff* masonry columns confined by  
 440 GFRCM is reported in Fig. 13 for all the tested columns. In general, a non-linear ascending branch can be  
 441 observed up to the peak stress, followed by a load drop. This loss of capacity after the peak stress corresponds  
 442 physically to the compressive crushing of the inner masonry and it is generally followed by a softening branch,  
 443 which is governed by the behavior of the damaged masonry inside the jacket. Exception is made for the  
 444 specimens confined with three layers tested by UniSal, which showed a limited load recovery before the failure  
 445 occurred. The extension of the post-peak branch depended on the number of applied textile layers. Specimens  
 446 confined with two and three layers of textile exhibited greater strength increases but, in some cases, lower  
 447 values of ultimate strain (more brittle behavior). The increase of the value of axial strain corresponding to peak  
 448 stress was equal to 56% for confinement with one and two layers, while it was equal to 18% for specimens  
 449 confined with three layers, considering the specimens tested by UniPa; the same quantities evaluated for  
 450 specimens tested at UniSal were equal to 120%, 1% and 156% for confinement with one layer, two and three  
 451 layers, respectively.

452 It was also observed that hoop strains were negligible up to the first cracking stress, and increased rapidly  
 453 afterwards; this confirms that confinement activates after the tensile strain of the masonry is reached. Hoop  
 454 strains were larger for specimens confined with more layers, showing the ability of a stiffer jacket to carry a

455 greater amount of hoop tensile force and consequently to provide greater values of confinement pressure, as  
456 expected.

457 It is worth noting that the two laboratories performed the tests with a different control, as described in the  
458 previous section. UniPa adopted displacement control, while UniSal performed tests under force control.  
459 Consequently, the measures of the strains in the post peak branch are different.



460 **Fig. 13. Axial stress vs. axial and hoop strain for Tuff masonry specimens confined by GFRCM systems. a) Specimens**  
461 **confined with one layer; b) Specimens confined with two layers; c) Specimens confined with three layers.**

462 The experimental results of Tuff masonry columns wrapped by GFRCM system are shown in Table 7.

463

Table 7. Experimental results for Tuff masonry columns strengthened by means of GFRCM systems

Outputs	Tuff											
	1 layer				2 layers				3 layers			
	UniPa		UniSal		UniPa		UniSal		UniPa		UniSal	
	3_R M	4_RM	3_R M	4_R M	5_R M	6_R M	5_R M	6_RM	7_RM	8_RM	7_R M	8_RM
<b>Max. stress [MPa]</b>	2.86	2.32	2.90	2.06	2.84	3.43	3.69	3.78	3.98	4.68	4.51	4.85
(Av.)	(2.59)		(2.48)		(3.14)		(3.74)		(4.33)		(4.68)	
<b>Max. axial strain [-]</b>	0.65	0.69	0.84	0.011 7	0.55	0.78	0.010 1	0.72	0.48	0.53	0.01 63	0.57
(Av.)	(0.67)		(0.0101)		(0.67)		(0.87)		(0.51)		(0.0110)	
<b>Ultimate stress [MPa]</b>	2.32	1.86	2.64	1.66	2.28	2.74	3.24	3.18	3.38	3.74	3.60	3.86
(Av.)	(2.09)		(2.15)		(2.51)		(3.21)		(3.56)		(3.73)	
<b>Ultimate axial strain [-]</b>	0.75	0.0227	0.010 1	0.028 3	0.014 1	0.011 6	0.011 2	0.0175	0.0140	0.0121	0.01 90	0.0169
(Av.)	(0.0151)		(0.0192)		(0.0129)		(0.0144)		(0.0131)		(0.0179)	
<b>Max. hoop strain [-]</b>	0.51	0.2	0.56	0.02	0.01	0.09	0.55	0.12	0.13	0.15	0.01 02	0.052
(Av.)	(0.26)		(0.29)		(0.05)		(0.34)		(0.14)		(0.54)	
<b>First cracking stress [MPa]</b>	1.01	1.36	1.18	0.99	1.35	1.30	0.55	2.49	3.09	1.60	3.65	3.26
(Av.)	(1.18)		(1.09)		(1.32)		(1.52)		(2.35)		(3.46)	
<b>Elastic modulus [MPa]</b>	1469	668	541	449	1082	1326	2586	632	1331	2855	939	1051
(Av.)	(1068)		(495)		(1204)		(1609)		(2093)		(995)	
$\sigma_{vmax,RM}/\sigma_{vmax,URM}$	1.13	0.91	1.14	0.81	1.12	1.35	1.45	1.48	1.56	1.84	1.77	1.91

465

### Tuff masonry columns confined by SRG

466

467

468

469

470

471

472

473

474

475

476

477

478

479

480

481

482

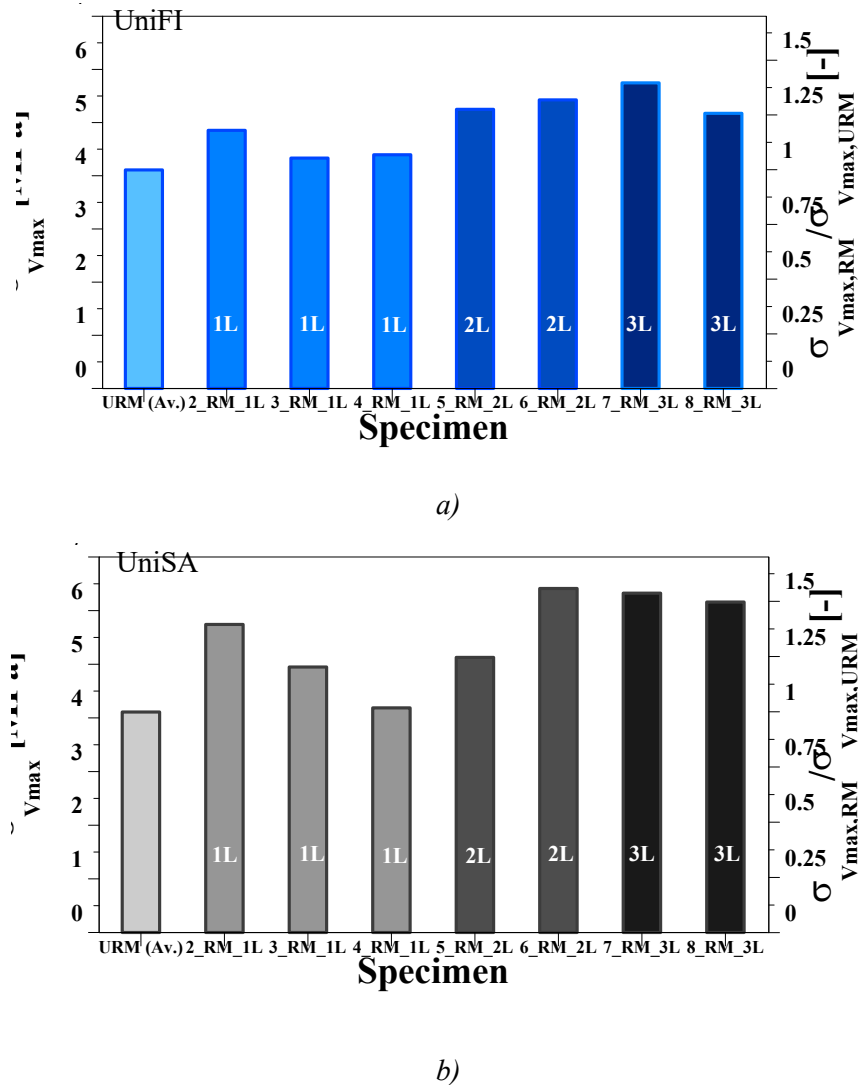
483



484 **Fig. 14. Failure mode of Tuff masonry specimens confined by SRG.**

485 Fig. 15 shows the maximum axial stress  $\sigma_{Vmax, RM}$  recorded during the test and the increase in load carrying  
 486 capacity for Tuff masonry specimens wrapped by SRG. The latter was evaluated as the ratio between  $\sigma_{Vmax, RM}$   
 487 and the average maximum stress,  $\sigma_{Vmax, URM}$  recorded in the two unreinforced columns tested by UniFi and  
 488 UniSa. The specimens wrapped by one layer had a limited average strength increase, equal to 10% for UniFi  
 489 and 21% for UniSa. More consistent enhancements were observed for specimens reinforced with two and three

490 layers. In particular, strength increase for samples tested at UniFi was equal to 30% and 33% for two and three  
 491 layers, while the corresponding values for columns tested at UniSa were equal to 40% and 52%, respectively.



492 **Fig. 15. Maximum stress and dimensionless load carrying capacity of Tuff masonry columns confined by SRG a)**  
 493 **Specimens tested by UniFi; b) Specimens tested by UniSa.**

494 It should be observed that the effect of SRG confinement is different from that detected for GFRCM; in fact,  
 495 the latter produced a higher increase of strength while for the former a significant increase of the deformation  
 496 capacity was registered.

497 The trend of the axial stress as a function of axial and hoop strains for SRG confined *Tuff* masonry columns is  
 498 reported in Fig. 16. The trend of these curves is initially linear up to the stress corresponding to first cracking.  
 499 This branch is followed by a load drop, in correspondence of the masonry crushing near the column ends. The  
 500 post-peak branch appeared to be dependent on the number of adopted layers of steel mesh. In particular, a  
 501 softening behavior, with a quick load drop, was shown by specimens confined with one layer, while a more  
 502 “ductile” behavior was recorded for specimens reinforced with two and three layers. The irregular trend of the  
 503 post-peak branch is connected with the extensive damage of the external jacket and masonry core,  
 504 characterized by diffuse cracking, slippage of the fabric and spalling of the matrix, in addition to the cracking  
 505 of the masonry core. It is remarkable that the ratio between the average value of axial strain at peak of confined  
 506 and unconfined columns, was equal to 14.3 and 16.8, for specimens tested by UniFi, respectively with two and  
 507 three layers. Concerning the samples tested at UniSa, the same ratios were equal to 7.3 and 20.4, confirming



508 that SRG confinement induces significant increments of deformation capacity, which could be interpreted as  
 509 pseudo-ductility.

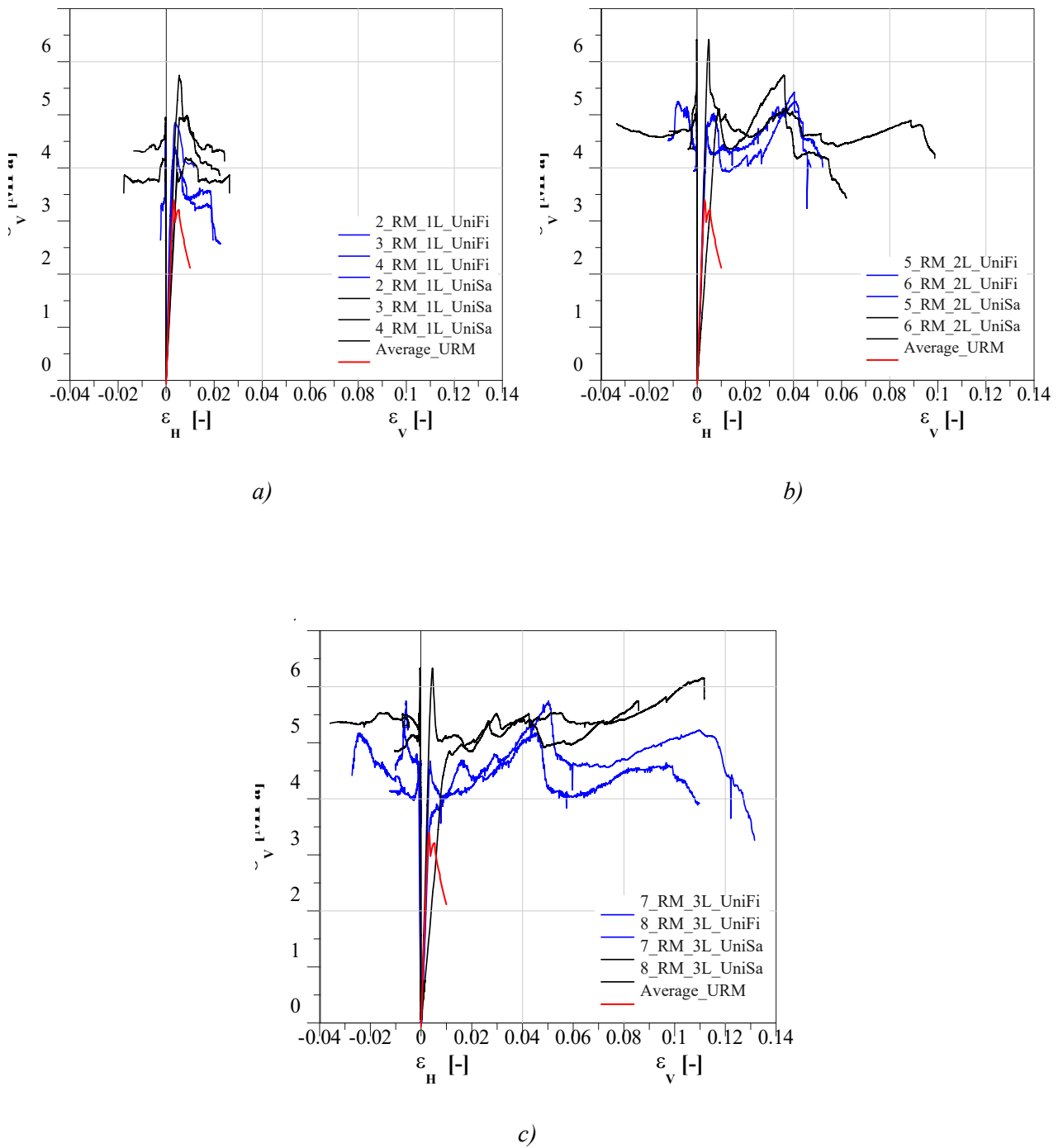


**Fig. 16. Axial stress vs. axial and hoop strain for Tuff masonry specimens confined by SRG. a) Specimens confined with one layer; b) Specimens confined with two layers; c) Specimens confined with three layers.**

510 Results recorded from tests on Tuff columns strengthened by SRG are reported in Table 8.

511

512 **Table 8. Experimental results for Tuff masonry columns strengthened by means of SRG systems.**

Outputs	Tuff													
	1 layer						2 layers				3 layers			
	UniFi		UniSa				UniFi		UniSa		UniFi		UniSa	
	2_R M	3_RM	4_RM	2_R M	3_RM	4_RM	5_R M	6_R M	5_R M	6_R M	7_R M	8_R M	7_R M	8_R M
<b>Max. stress [MPa]</b>	4.85	4.33	4.39	5.74	4.95	4.19	5.25	5.43	5.13	6.41	5.75	5.18	6.30	6.16
(Av.)	(4.52)		(4.96)				(5.34)		(5.77)		(5.47)		(6.23)	
<b>Max. axial strain [-]</b>	0.37	0.39	0.38	0.55	0.56	0.82	0.04 09	0.04 03	0.03 67	0.48	0.05 02	0.04 50	0.45	0.11 11
(Av.)	(0.38)		(0.64)				(0.0406)		(0.0208)		(0.0476)		(0.0578)	
<b>Ultimate stress [MPa]</b>	4.02	3.44	3.51	-	-	-	-	-	-	-	-	-	-	-
(Av.)	(3.65)		-				-		-		-		-	
<b>Ultimate axial strain [-]</b>	4.59	4.13	3.53	-	-	-	-	-	-	-	-	-	-	-
(Av.)	(4.08)		-				-		-		-		-	
<b>Max. hoop strain [-]</b>	0.02	0.02	0.02	-	0.01	0.04	0.02	0.02	0.04	0.02	0.01	0.01	0.04	0.03
(Av.)	(0.02)		(0.03)				(0.02)		(0.03)		(0.01)		(0.04)	
<b>First cracking stress [MPa]</b>	2.69	2.79	1.58	1.43	2.10	2.50	3.74	3.80	4.53	5.36	3.40	4.46	5.13	4.11
(Av.)	(2.35)		(2.01)				(3.77)		(4.95)		(3.93)		(4.62)	
<b>Elastic modulus [MPa]</b>	131 5	1894	2069	137 0	1757	925	1210	1076	619	110 2	993	1217	148 5	492
(Av.)	(1759)		(1341)				(1143)		(860)		(1105)		(989)	
$\sigma_{vmax,RM}/\sigma_{vmax,URM}$	1.18	1.05	1.07	1.40	1.20	1.02	1.28	1.32	1.25	1.56	1.40	1.26	1.54	1.50

513 **Unreinforced clay masonry**

514 Fig. 17 shows the typical failure modes of unreinforced clay brick masonry columns tested by the four  
 515 laboratories UniBo, UniCal, PoliMi, UniNa.

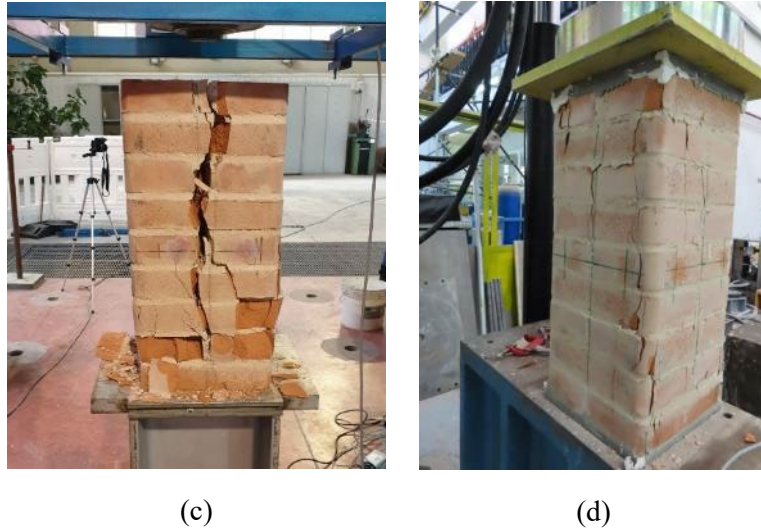
516



(a)

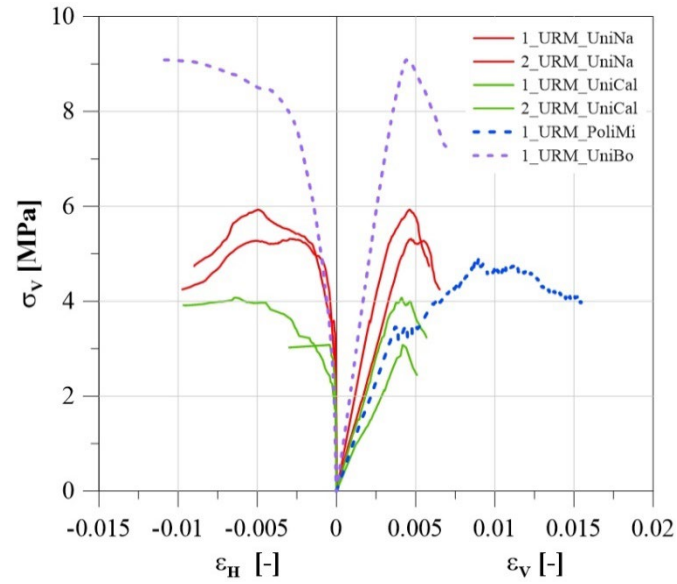


(b)



517 **Fig. 17. Unreinforced clay brick masonry specimens after testing: a) 1\_URM PoliMi; b) 2\_URM UniBo; c) 1\_URM**  
 518 **UniCal; d) 1\_URM UniNa .**

519 All URM specimens showed similar failure modes, characterized by sub-vertical cracks developed along the  
 520 longitudinal direction. Only the specimen tested by PoliMi (Fig. 17a) showed a slightly different failure mode.  
 521 In particular, the crack appears to be more limited in a specific portion of masonry. This difference is probably  
 522 due to lack of top and bottom capping layers. In fact, localized premature failures are enhanced without a  
 523 regular top and bottom surface. Fig. 18 shows the axial stress as a function of the longitudinal and hoop strains  
 524 experimentally obtained for the URM columns.



525  
 526 **Fig. 18. Axial stress vs. axial and hoop strain for unreinforced clay brick masonry specimens.**

527 Different repetitions of URM masonry columns have been considered for experimental tests by the four labs.  
 528 One URM specimen was tested by PoliMi and UniBo (dotted curves of Fig. 18); while, two URM specimens  
 529 were tested by UniNa and UniCal (solid curves of Fig. 18). The different behavior of the URM specimen tested  
 530 by the PoliMi can be found also by observing the stress-strain law (Fig. 18). In particular, the specimen showed  
 531 a conventional ultimate strain equal to 15.5% (dotted blue curve of Fig. 18), significantly higher than values  
 532 achieved by the other URM columns (average value of 5.9%). The load carrying capacities of URM specimens

533 resulted compatible with the typical dispersion of masonry material. The columns manufactured at UniBo  
 534 exhibited minimum and maximum axial stress values equal to 4.92 MPa and 9.09 MPa respectively.  
 535 Conversely, for the specimens manufactured at UniSal the maximum axial stress ranges from 3.08 MPa to  
 536 5.93 MPa. The URM specimens tested by the UniCal lab have maximum axial stress about 35% lower than  
 537 URM specimens tested by UniNa, but they did not test the specimens with the capping.

538 The URM specimens manufactured by UniBo (Fig. 18) show a variable initial stiffness, from 714 to 2391  
 539 MPa. Again, the minimum value was detected for the specimen tested by the PoliMi lab, for which no capping  
 540 was realized, as already discussed (Fig. 17). For these specimens, the top and bottom surfaces were not  
 541 regularized. In fact, the initial average stiffness is very close between the specimen tested by PoliMi and UniCal  
 542 (blue curve of Fig. 18). Specimens tested by UniNa showed an average initial stiffness of about 1400 MPa.  
 543 Full experimental results are reported in Table 9.

544 **Table 9. Experimental results for unreinforced clay masonries.**

Outputs	UniNa		UniCal		PoliMi	UniBo
	1_URM	2_URM	1_URM	2_URM	1_URM	1_URM
<b>Maximum stress [MPa]</b>	5.93	5.31	3.08	4.07	4.92	9.09
(Av.)	(4.60)				(7.01)	
<b>Maximum axial strain [-]</b>	0.46	0.47	0.42	0.41	0.80	0.44
(Av.)	(0.44)				(0.62)	
<b>Ultimate stress [MPa]</b>	4.74	4025	2.38	3.15	4.42	7.26
(Av.)	(3.63)				(5.84)	
<b>Ultimate axial strain [-]</b>	0.58	0.65	0.51	0.57	-	0.69
(Av.)	(0.58)				-	
<b>Maximum hoop strain [-]</b>	0.49	0.30	0.04	0.63	-	1.13
(Av.)	(0.37)				-	
<b>First cracking stress [MPa]</b>	3.55	2.69	2.05	1.47	3.48	-
(Av.)	(2.44)				(3.48)	
<b>Elastic modulus [MPa]</b>	1674	1173	714	1064	809	2391
(Av.)	(1156)				(16)	

545 **Clay masonry confined by Glass Textile Reinforced Mortar (GFRCM)**

546 The specimens wrapped by inorganic matrix-glass grid composites were manufactured by UniSal and later  
 547 tested by UniNa and UniCal. The failure modes of the strengthened masonry columns are shown in Fig. 19.  
 548 As seen for *Tuff* columns, the failure of the confined columns occurs when the tensile capacity of the fibres is  
 549 reached, usually around the corner regions. In some cases the failure was also accompanied by buckling and  
 550 debonding phenomena at mid height, along the vertical direction. This buckling phenomenon can be due to  
 551 the shear stress developing at the ends of the specimen through the bond between the masonry and the external  
 552 wrap.

553

554

555

556

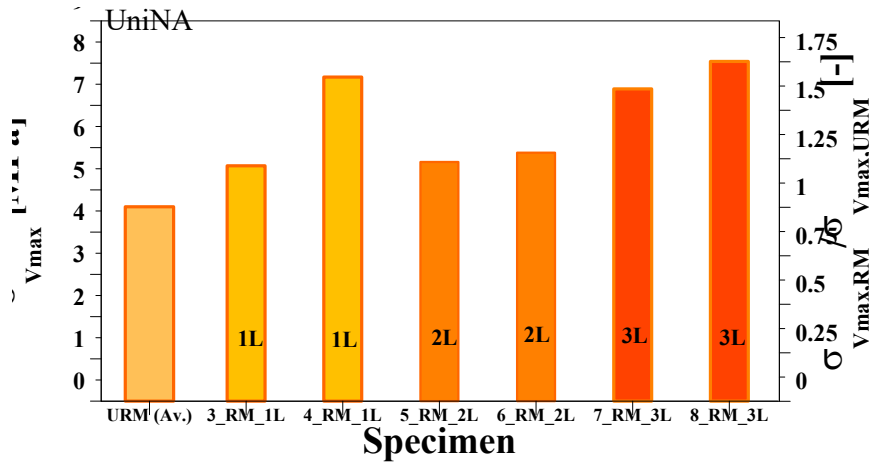
557



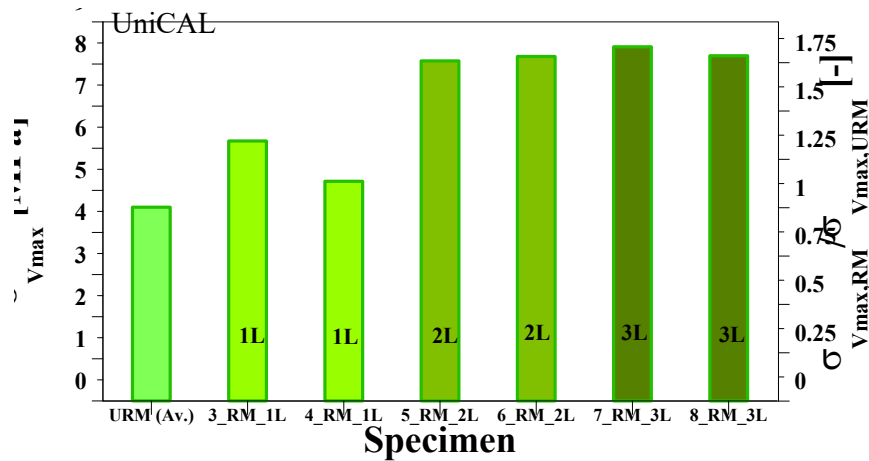
559 *Fig. 19. Failure mode of clay masonry specimens confined by GFRCM.*

560

561 The increase of load carrying capacity, for all the considered cases, is reported in Fig. 20.



a)



b)

562 Fig. 20. Maximum stress and dimensionless load carrying capacity of clay bricks masonry columns confined by  
 563 GFRCM a) Specimens tested by UniNa; b) Specimens tested by UniCal.

564 Full experimental results are shown in Table 10.

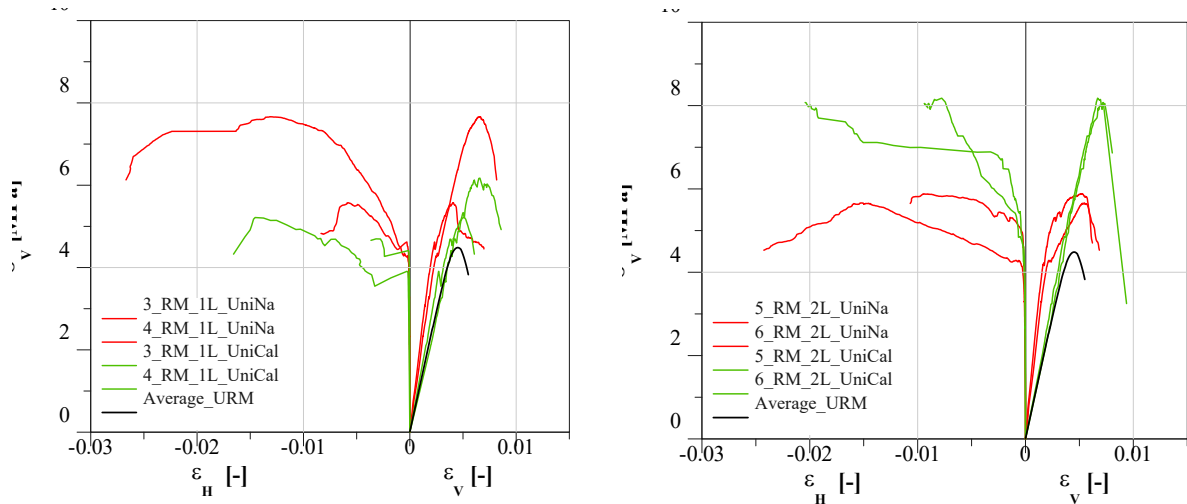
565 Table 10. Experimental results for clay brick masonry columns strengthened by means of GFRCM systems.

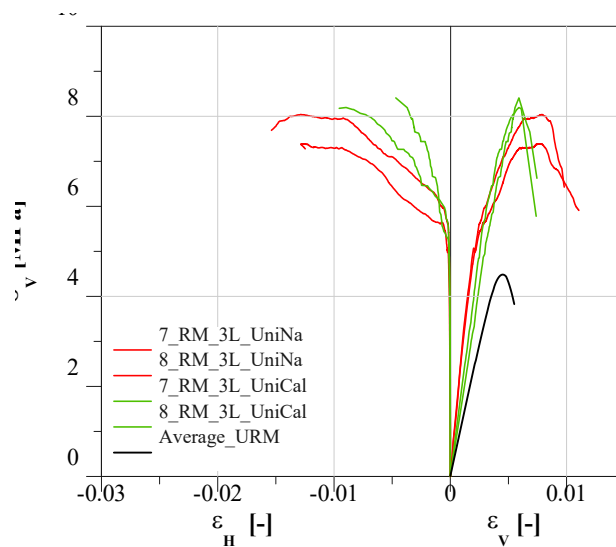
Outputs	Clay bricks											
	1 layer				2 layers				3 layers			
	UniNa		UniCal		UniNa		UniCal		UniNa		UniCal	
	3_R M	4_RM	3_RM	4_RM	5_RM	6_R M	5_RM	6_R M	7_RM	8_RM	7_R M	8_R M
Max. stress [MPa]	5.57	7.67	6.17	5.22	5.66	5.88	8.07	8.18	7.39	8.04	8.41	8.20

(Av.)	(6.62)	(5.70)	(5.77)	(8.13)	(7.72)	(8.31)						
<b>Max. axial strain [-]</b>	0.41	0.66	0.66	0.51	0.55	0.53	0.72	0.67	0.77	0.79	0.59	0.59
(Av.)	(0.54)	(0.59)	(0.54)	(0.70)	(0.78)	(0.59)						
<b>Ultimate stress [MPa]</b>	4.45	6.13	4.78	4.21	4.53	4.70	6.28	6.67	5.91	6.43	6.44	5.62
(Av.)	(5.29)	(4.50)	(4.62)	(6.48)	(6.17)	(6.03)						
<b>Ultimate axial strain [-]</b>	0.70	0.82	0.86	0.61	0.69	0.62	0.80	0.80	0.011	0.98	0.74	0.74
(Av.)	(0.76)	(0.73)	(0.65)	(0.80)	(0.0104)	(0.74)						
<b>Max. hoop strain [-]</b>	0.58	0.013	0.024	0.014	0.015	0.95	0.020	0.78	0.012	0.012	0.47	0.90
(Av.)	(0.95)	(0.0197)	(0.0124)	(0.0141)	(0.0127)	(0.69)						
<b>First cracking stress [MPa]</b>	3.072	3.28	2.07	2.04	3.30	4.19	2.58	3.01	5.04	5.63	3.01	3.06
(Av.)	(3.18)	(2.06)	(3.75)	(2.80)	(5.34)	(3.04)						
<b>Elastic modulus [MPa]</b>	2202	1858	1082	1398	2254	2755	1245	1340	2926	2669	1637	1925
(Av.)	(2030)	(1240)	(2505)	(1293)	(2798)	(1781)						
$\sigma_{vmax,RM}/\sigma_{vmax,URM}$	1.23	1.69	1.32	1.11	1.24	1.29	1.73	1.75	1.62	1.77	1.80	1.75

566

567 The behavior of confined specimens in terms of peak load is reported in Fig. 20. The effectiveness of wrapping  
568 reinforcement becomes more apparent for two- and three-layers cases for columns tested by UniCal, while for  
569 tests carried out by UniNa lower variation of the peak-load have been obtained varying the number of layers.  
570 However, the behavior of confined specimens (Fig. 20) is characterized by a strong dispersion in terms of load  
571 carrying capacity, which reduces as the amount of confining reinforcement increases. Fig. 21 shows  
572 experimental curves in terms of axial stress vs axial and transverse strains for all the tested specimens. After  
573 the peak stress, all the columns showed a brittle softening behavior.





574

575 **Fig. 21. Axial stress vs. axial and hoop strain for clay brick masonry specimens confined by GFRCM systems. a)**  
 576 **Specimens confined with one layer; b) Specimens confined with two layers; c) Specimens confined with three layers.**

577 The results obtained by UniNa (red curves of Fig. 21) showed significant issues related to the efficiency of the  
 578 strengthening system. In particular, low number of layers could lead to poor confinement performance. It has  
 579 been confirmed by the strong dispersion detected for columns confined by 1-layer of GFRCM. The maximum  
 580 axial stress ranges from 5.57 MPa to 7.67 MPa (red curves Fig. 21a) where, the first value is very similar to  
 581 the capacity of URM specimens, while the second is comparable with the specimen confined by 3-layers  
 582 (red curves Fig. 21c). For specimens strengthened with 2-layers system, the load carrying capacity results weakly  
 583 increased (5.66 and 5.88 MPa) (red curves of Fig. 21b) with respect to that of unconfined specimens.  
 584 Conversely, the 3-layers systems showed a clear beneficial effect in terms of load carrying capacity (7.39 and  
 585 8.04 MPa).

586 The specimens tested by UniCal exhibited an almost constant load carrying capacity for specimens reinforced  
 587 with 2 and 3 layers (green curves in Fig. 21b and c). The specimens confined with 1-layer system (orange  
 588 curves in Fig. 21a) present a maximum axial stress ranging from 5.22 MPa to 6.17 MPa while, the average  
 589 value of other strengthened columns (2 and 3-layers system) is 8.2 MPa.

590 As also observed for the strength values, the elastic modulus (Fig. 21) reduces its dispersion by increasing the  
 591 reinforcement amount. The stiffness of specimens tested by UniCal (green curves of Fig. 21) appears always  
 592 lower than that of specimens tested by UniNa (red curves of Fig. 21). Experimental results showed average  
 593 values of 2030, 2505 and 2800 MPa for the specimens tested by UniNa with one-, two- and three-layers'  
 594 system, respectively. Conversely, the specimens tested by UniCal are characterized by an average stiffness of  
 595 1240, 1293 and 1781 MPa. As expected, the elastic modulus progressively increases with the amount of  
 596 reinforcement, due to the additional contribution of composite and the reduced capacity of lateral expansion.

597 The ultimate longitudinal axial strain of specimens tested by UniCal appears to be weakly influenced by the  
 598 amount of reinforcement (approximately 7‰ – green curves of Fig. 21). However, this aspect is probably due  
 599 to the smaller reliability of measurements of the axial displacement after the attainment of the peak stress. In  
 600 fact, for the confined columns, the LVDT devices were placed on the wrapped surface; therefore, especially  
 601 once the peak-state was exceeded, a probable slip between the internal masonry and composite may promote  
 602 measurement errors. This effect is less marked for axial deformations at the peak stress

603 The ultimate deformations detected for the specimens tested by UniNa (Fig. 21) confirmed what was  
 604 highlighted by the analysis of the peak loads. The two unreinforced specimens and one specimen strengthened



605 with a one-layer system exhibited very similar behavior while the remaining specimen strengthened with one-  
606 layer system, showed properties very close to specimens reinforced with three-layers system. Very small  
607 increases in capacity were also detected for systems reinforced with two layers, with respect to the unreinforced  
608 specimens. The three-layer systems instead showed a clear beneficial effect in terms of load capacity.

609 The maximum hoop strains at the peak load reduce as the number of layers increases (Fig. 21).

610 ***Clay masonry confined by Steel Reinforced Grout (SRG)***

611 Clay brick masonry columns strengthened by SRG reinforcement were tested by UniBo and PoliMi, while  
612 they were all manufactured by UniBo. Fig. 22 shows the failure modes observed for the confined columns.  
613 The failure modes resulted very similar for all the tested samples (Fig. 22). The damage started from the edges  
614 for all specimens. Once the peak stress was exceeded, the external layer of the strengthening system showed a  
615 debonding phenomenon from the substrate or from the inner layer. This mechanism was observed starting  
616 from mid height of the wrapped surfaces (along the longitudinal axis).

617

618

*Specimen tested by PoliMi*

*Specimen tested by UniBo*

*One layer  
SRG*



*Two layers  
SRG*



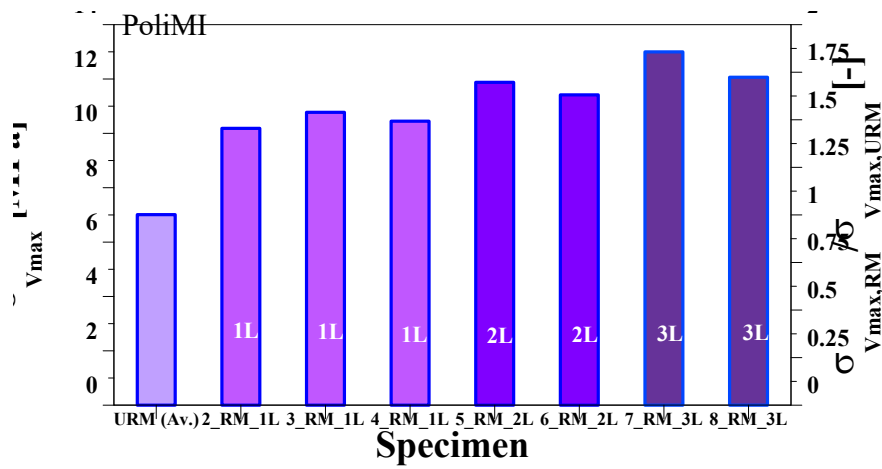
Three layers  
SRG



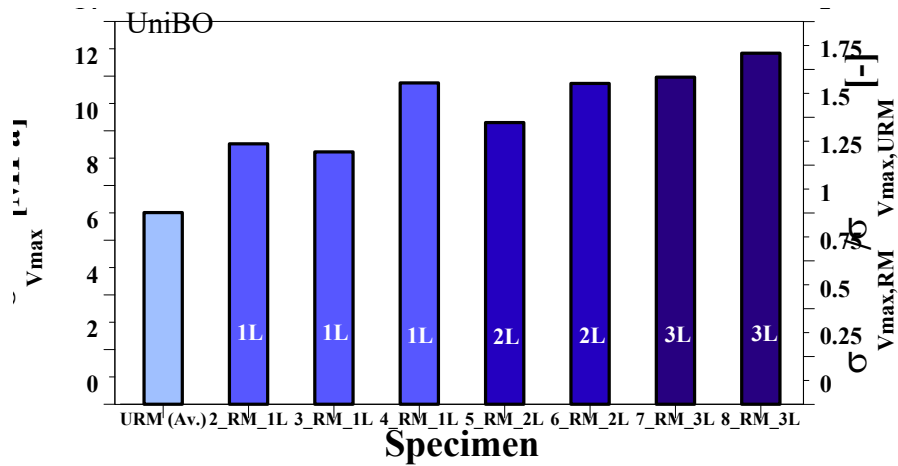
619 *Fig. 22. Failure mode of clay brick masonry specimens confined by SRG.*

620 Fig. 23 shows the increase in peak-stress of the confined masonry columns. Effectiveness of the wrapping  
 621 system increases with the number of layers. It is also clear that the dispersion of results decreases with the  
 622 amount of reinforcement.

623



a)

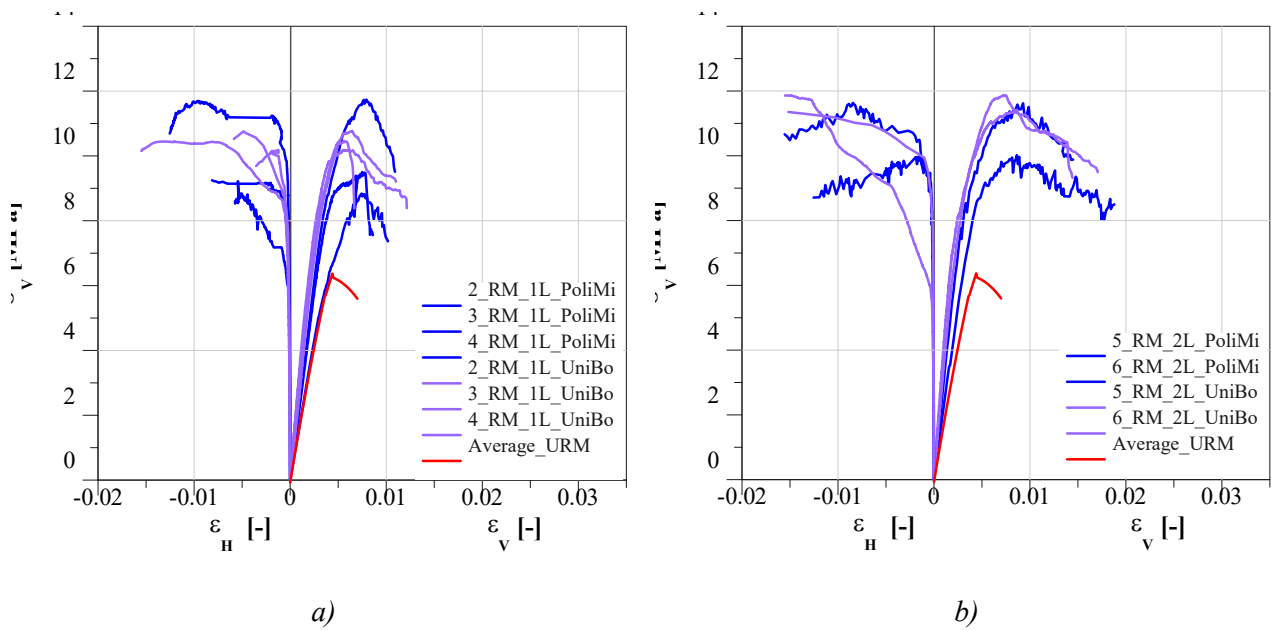


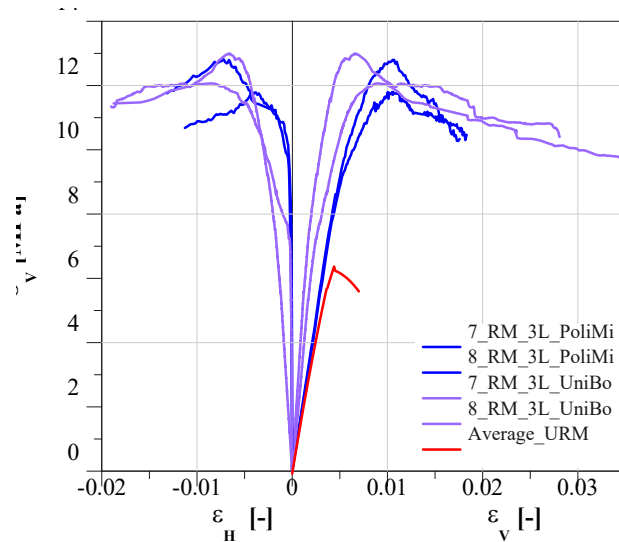
b)

624 Fig. 23. Maximum stress and dimensionless load carrying capacity of clay bricks masonry columns confined by SRG  
 625 a) Specimens tested by PoliMi; b) Specimens tested by UniBo.

626 Furthermore, it is interesting to observe the complete axial stress-strain curve of each specimen and for the  
 627 different number of layers (Fig. 24).

628





c)

629 **Fig. 24. Axial stress vs. axial and hoop strain for clay masonry specimens confined by SRG. a) Specimens confined**  
 630 **with one layer; b) Specimens confined with two layers; c) Specimens confined with three layers.**

631 Curves become smoother by increasing the number of layers. In fact, the specimens wrapped by three-layers  
 632 present a similar load carrying capacity and initial stiffness. For masonry columns wrapped by one-layer  
 633 system the maximum axial stress ranges from 9.23 MPa (PoliMi) to 11.77 MPa (UniBo). Increasing the amount  
 634 of fabric plies, the maximum axial stress ranges from 10.3 MPa (PoliMi) to 11.88 MPa (UniBo) and from  
 635 11.96 (PoliMi) to 13 MPa (UniBo) for two- and three-layer systems, respectively. The experimental tests  
 636 carried out by UniBo (violet curves of Fig. 21) show a dispersion lower than the results by PoliMi. In fact,  
 637 both the load carrying capacity and the ultimate strains values progressively increase with the number of layers.  
 638 These results are affected by a small difference between one specimen and the other of the same type.

639 The initial stiffness values are more uniform if compared with those of the URM specimens. Experimental  
 640 results showed average values of 2157, 2488 and 1901 MPa for the specimens tested by PoliMi with one-,  
 641 two- and three-layers system, respectively. While the corresponding specimens tested by UniBo are  
 642 characterized by an increasing average stiffness of 3365, 3702 and 3948 MPa. For these specimens, the  
 643 equivalent elastic modulus seems to be weakly influenced by the strengthening system if compared with the  
 644 specimens tested by PoliMi.

645 The specimens tested by UniBo, especially the 3-layer systems, have shown higher ultimate axial deformations  
 646 with respect to those columns tested by PoliMi. The longitudinal strain, at the maximum axial stress, seems  
 647 generally not influenced by the number of layers. On the other hand, the ultimate strain clearly increases with  
 648 the amount of reinforcement ratio.

649 The axial stress-hoop strain curves (left part of graphs in Fig. 24) are probably affected by measurement issues  
 650 due to the post-cracked state. However, the beneficial effect of confinement due to the composite is clear. The  
 651 experimental results for clay masonry columns confined by means of SRG systems are shown in Table 11.

652

653

654 **Table 11. Experimental results for clay brick masonry columns strengthened by means of SRG systems.**

Outputs	Clay bricks													
	1 layer				2 layers				3 layers					
	PoliMi		UniBo		PoliMi		UniBo		PoliMi		UniBo			
	2_R M	3_R M	4_R M	2_R M	3_R M	4_R M	5_R M	6_R M	5_R M	6_R M	7_R M	8_R M	7_R M	8_R M
<b>Max. stress [MPa]</b>	9.52	9.23	11.7	10.1	10.7	10.4	10.3	11.7	11.8	11.4	11.9	12.8	13.	12.0
<i>(Av.)</i>	(10.17)		(10.47)		(11.02)		(11.65)		(12.40)		(12.53)			
<b>Max. axial strain [-]</b>	0.78	0.84	0.81	0.56	0.64	0.56	0.88	0.90	0.72	0.86	0.01	0.01	0.66	0.91
<i>(Av.)</i>	(0.81)		(0.59)		(0.89)		(0.79)		(0.0104)		(0.79)			
<b>Ultimate stress [MPa]</b>	7.56	7.32	9.34	8.32	9.25	8.38	8.16	9.34	9.38	9.06	10.4	10.3	10.3	9.46
<i>(Av.)</i>	(8.07)		(8.65)		(8.75)		(9.22)		(10.38)		(9.91)			
<b>Ultimate axial strain [-]</b>	0.87	0.01	0.01	0.12	0.01	0.67	0.01	0.01	0.01	0.01	0.01	0.01	0.02	0.03
<i>(Av.)</i>	(0.0103)		(0.99)		(0.0168)		(0.0158)		(0.0180)		(0.0316)			
<b>Max. hoop strain [-]</b>	0.01	0.54	0.85	0.12	0.49	0.01	0.18	0.85	0.01	0.01	0.35	0.75	0.52	0.87
<i>(Av.)</i>	(0.86)		(0.61)		(0.52)		(0.0150)		(0.55)		(0.70)			
<b>First cracking stress [MPa]</b>	5.34	5.07	8.81	-	-	-	3.53	6.17	-	-	9.76	7.81	-	-
<i>(Av.)</i>	(6.41)		-		(4.85)		-		(8.79)		-			
<b>Elastic modulus [MPa]</b>	23	1731	2441	3983	2936	3177	2097	2879	3342	4061	1869	1933	4647	3248
<i>(Av.)</i>	(2157)		(3365)		(2488)		(3702)		(1901)		(3948)			
$\sigma_{Vmax, RM} / \sigma_{Vmax, URM}$	1.44	1.54	1.49	1.36	1.32	1.68	1.67	1.60	1.47	1.67	1.85	1.69	1.71	1.83

655

656

657 **DESIGN CONSIDERATION**

658 As evidenced by the above described experimental results, the axial response of a FRM-confined masonry  
659 column is affected by cracks opening both into the core and within the jacket. For this reason, the analytical  
660 prediction of the axial strength cannot disregard the parameter related to the masonry, the fabric and the  
661 FRM-matrix. All analytical models proposed so far to predict the axial strength of the FRM confined  
662 masonry columns were developed according to this consideration; among those, the models by Krevaiakas [47],  
663 Ramaglia et al. [54], Cascardi et al. [43], Italian CNR DT-215 [32] and ACI 549-R13 [15] guidelines. Even if  
664 derived from different approaches, the formulations proposed to predict the axial strength of confined masonry  
665 columns present a similar non-linear form. The main difference between the mentioned model predictions is  
666 related to the computation of the effective confinement pressure [55].

667 In the following, the Standards available to date, namely the Italian CNR DT 215 [32] and the American  
668 ACI549-R13 [15], are used for comparison with experimental results, in order to further check the  
669 effectiveness of the design relationship proposed for the confinement of masonry columns, mostly when the  
670 number of layers increases, considering that the already available experimental database on this aspect is very  
671 limited. The analytical formulations of the two models are summarized in Table 12.

672

673

674 **Table 12. Comparison of the prediction models.**

	ACI 549-R13 [15]	CNR DT 215 [32]
<b>Compressive strength of the FRCM-confined column</b>	$f_{mcd} = f_{md} + 3.1 k_a f_i$	$f_{mcd} = f_{md} \left[ 1 + k' \left( \frac{k_H f_{l,eff}}{f_{md}} \right)^{\alpha_1} \right]$
<b>k'</b>	-	$k' = \alpha_2 \left( \frac{g_m}{10} \right)^{\alpha_3}$
<b>Shape factor</b>	$k_a = \frac{A_e}{A_c} \left( \frac{b}{h} \right)^2$	-
	$\frac{A_e}{A_c} = 1 - \frac{\left[ \left( \frac{b}{h} \right) (h - 2r_c)^2 + \left( \frac{h}{b} \right) (h - 2r_c)^2 \right]}{3bh}$	
<b><math>\alpha_1</math></b>	-	0.5
<b><math>\alpha_2</math></b>	-	1.0
<b><math>\alpha_3</math></b>	-	1.0
<b>Maximum confinement pressure</b>	$f_i = \frac{2nA_f E_f \varepsilon_{fe}}{\sqrt{b^2 + h^2}}$	
<b>Effective confinement pressure</b>	-	$f_{l,eff} = \frac{2nt_f E_f \varepsilon_{fe}}{\sqrt{b^2 + h^2}}$
<b>Horizontal geometrical efficiency coefficient</b>	-	$k_H = 1 - \frac{(b - 2r_c)^2 + (h - 2r_c)^2}{3bh}$
<b>Effective strain</b>	$\varepsilon_{fe} = \varepsilon_{fd} \leq 0.012$	$\varepsilon_{fe} = \min \left( k_{mat} \eta_a \frac{\varepsilon_u}{\gamma_m}; 0.4 \right)$
<b>FRCM-matrix efficiency coefficient</b>	-	$k_{mat} = 1.81 \left( \rho_{mat} \frac{f_{c,mat}}{f_{md}} \right)^2$
<b>Geometrical percentage of FRCM-matrix</b>	-	$\rho_{mat} = \frac{4t_{mat}}{\sqrt{b^2 + h^2}}$

675

676

677

678

679

680

681

682

683

684

685

686

687

688

689

690

691

692

693

694

For all tested specimens, the comparison between experimental results and predictions of the considered models in terms of maximum axial stress,  $f_{c,m}$ , are summarized in Tables 13-16 and Figs 25 and 26. Since the analytical relationships and predictions are used for comparison with experimental findings, the parameters introduced are the average values experimentally obtained and safety coefficients are not considered, thus the subscript “d” has been omitted for the utilized symbols.

Table 13 reports results obtained for the *Tuff* columns confined by GFRM systems. The analysis of the results ensures that both models provide similar predictions for each confinement configuration, i.e. for each confinement ratio ( $A_f/A_c$ ). For *Tuff* columns confined with one layer of GFRM the predicted  $f_{c,m}$  values are on average 12% and 16% higher than provide experimental ones, respectively for the CNR DT215 and ACI 549-R13 models. Referring to the specimens with three layers of GFRM the experimental values are on average underestimated of about 20%. Generally, the two models provide accurate predictions in case of one- and two- layer systems, considering the scattering of the experimental results (CoV=16% and 12% for one- and two- layer systems, respectively), while they appear both conservative for the case of three- layers’ configuration (CoV=8%).

695  
696

Table 13. *Tuff* masonry columns strengthened by GFRM systems: predicted/experimental comparison

Outputs	<i>Tuff</i>					
	1 layer		2 layers		3 layers	
	UniPa	UniSal	UniPa	UniSal	UniPa	UniSal
Experimental [MPa] (Av.)	2.59	2.48	3.14	3.74	4.33	4.68
Predicted CNR DT 215 [MPa]	2.82		3.14		3.30	
Pred./Exp. CNR DT215	1.09	1.14	1.	0.84	0.76	0.70
Predicted ACI 549-R13 [MPa]	2.86		3.28		3.71	
Pred./Exp. ACI 549- R13 [-]	1.12	1.19	1.05	0.88	0.86	0.79

697

698 The results of the comparison obtained for the *Tuff* columns confined by SRG systems are summarized in  
699 Table 14. For these columns the values of  $f_{c,m}$  predicted by the ACI model are higher than those predicted by  
700 the DT 215 model. The difference between the predictions of the two models is increasing with the number of  
701 confining layers.

702 In particular, for *Tuff* columns confined by one layer of SRG the predicted  $f_{c,m}$  values are on average 5% and  
703 22% higher than experimental ones for the DT215 and ACI 549-R13 models, respectively. The ratio between  
704 the predicted values and experimental results increases with the number of confining layers; referring to DT  
705 215 it results on average equal to 1.05 and 1.08 for columns confined by two- and three layers, respectively,  
706 while using the ACI model it is on average 1.33 and 1.54 for *Tuff* columns confined with 2 and 3 layers of  
707 SRG. As a consequence, predictions of the DT 215 model seem more accurate, considering that the CoV values  
708 of experimental results are 12%, 10% and 8% for one-, two- and three-layer systems, respectively.  
709

710

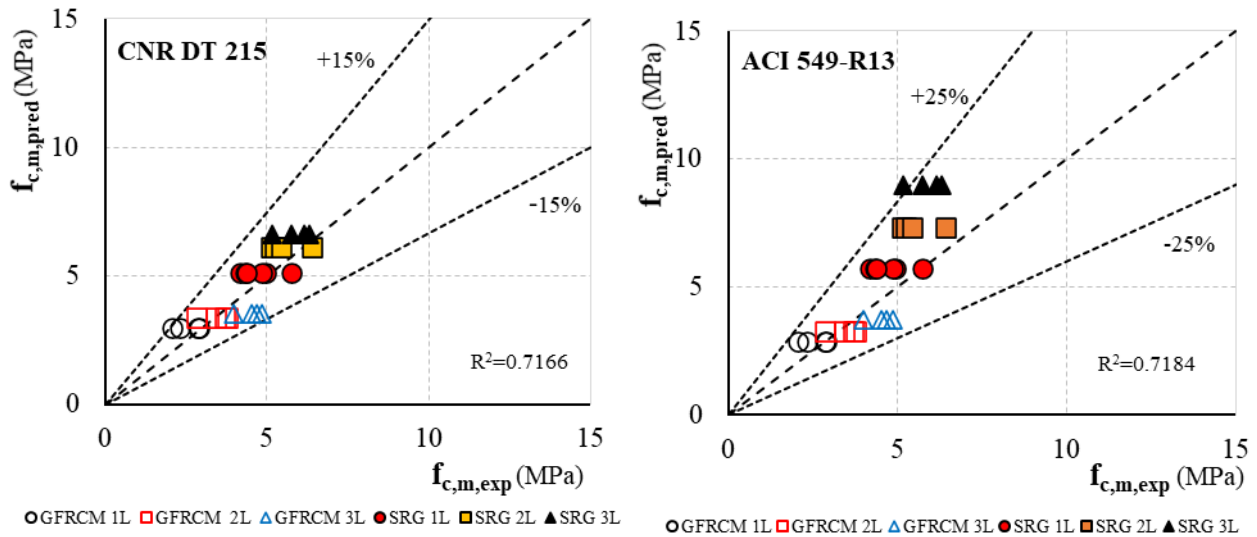
Table 14. *Tuff* masonry columns strengthened by SRG systems: predicted/experimental comparison

711

Outputs	<i>Tuff</i>					
	1 layer		2 layers		3 layers	
	UniFi	UniSa	UniFi	UniSa	UniFi	UniSa
Experimental [MPa] (Av.)	4.52	4.96	5.34	5.77	5.47	6.23
Predicted CNR DT 215 [MPa]	4.97		5.89		6.29	
Pred./Exp. CNR DT215	1.10	1.	1.10	1.02	1.15	1.01
Predicted ACI 549-R13 [MPa]	5.73		7.35		8.96	
Pred./Exp. ACI 549- R13 [-]	1.27	1.17	1.37	1.30	1.64	1.44

712

713 The comparison between predictions and experimental results for all tested *Tuff* columns is also illustrated in  
714 Fig. 25, where the above considerations are clearly confirmed.



715

716 *Fig. 25. Tuff masonry columns: predicted/experimental comparison*

717

718 The comparison between model predictions and experimental results for the clay brick columns confined by  
 719 GFRCM systems is summarized in Table 15. The obtained results show that the values of  $f_{c,m}$  predicted by  
 720 both considered models are similar and underestimate the experimental ones. However, considering the scatter  
 721 of experimental results the two models appear highly conservative only for the three-layer configuration  
 722 (COV= 18%, 20% and 5% for one-layer, two-layers and three-layers configuration, respectively).

723 *Table 15. Clay brick masonry columns strengthened by means of GFRCM systems: predicted/experimental comparison*

Outputs	Clay bricks					
	1 layer		2 layers		3 layers	
	UniNa	UniCal	UniNa	UniCal	UniNa	UniCal
Experimental [MPa] ( <i>Av.</i> )	6.62	5.70	5.77	8.13	7.72	8.31
Predicted CNR DT215 [MPa]	4.92		5.29		5.73	
Pred./Exp. CNR DT 215 [-]	0.76	0.83	0.91	0.65	0.74	0.69
Predicted ACI 549-R13 [MPa]	5.02		5.44		5.86	
Pred./Exp. ACI 549-R13 [-]	0.78	0.85	0.94	0.67	0.76	0.71

724

725 Table 16 summarizes the comparison between models' predictions and experimental results for clay brick  
 726 columns confined by SRG systems. For these columns the average values of the ratio predicted/experimental  
 727 results provided by the DT215 model is almost constant for each confinement ratio (0.75 for specimens  
 728 confined with one, two and three layers of SRG). The predictions of the ACI model become more accurate  
 729 with the number of confining layers; in fact, the ratio predicted/experimental results, is 0.83, 0.88 and 0.95 for  
 730 specimens confined with one, two and three layers of SRG, respectively.

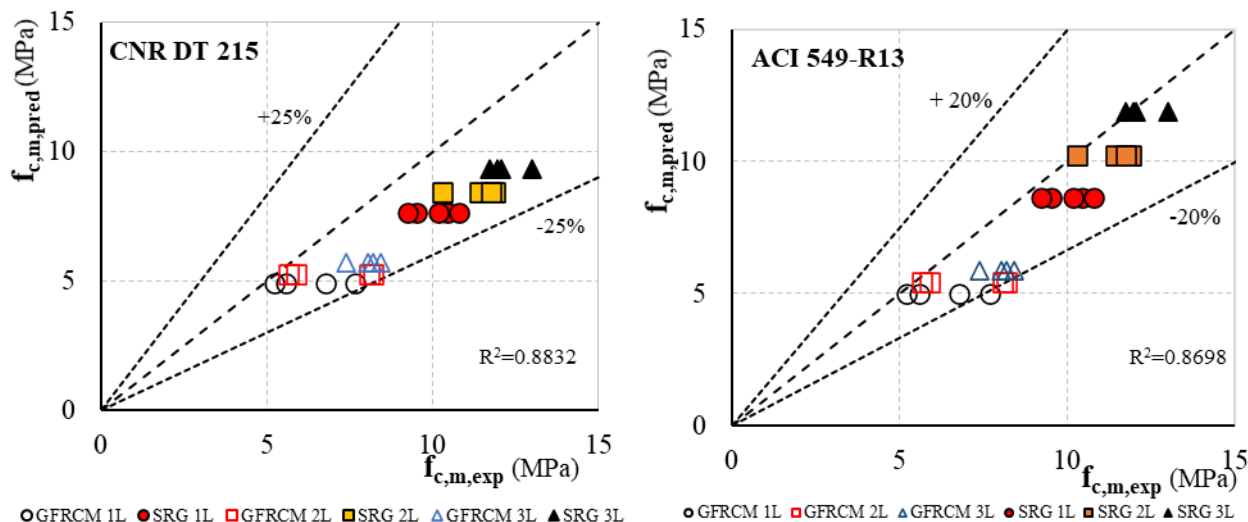
731 *Table 16. Clay brick masonry columns strengthened by means of SRG systems: predicted/experimental comparison*

Outputs	Clay bricks					
	1 layer		2 layers		3 layers	
	PoliMi	UniBo	PoliMi	UniBo	PoliMi	UniBo
Experimental [MPa] ( <i>Av.</i> )	10.17	10.47	11.02	11.65	12.40	12.53
Predicted CNR DT 215 [MPa]	7.67		8.42		9.32	
Pred./Exp. CNR DT 215 [-]	0.76	0.74	0.77	0.73	0.75	0.74
Predicted ACI 540-R13 [MPa]	8.62		10.24		11.86	



Pred./Exp ACI 549-R13 [-]	0.86	0.83	0.93	0.88	0.96	0.95
---------------------------	------	------	------	------	------	------

732 Fig. 26 reports the results of the comparison between predictions and experimental results for all tested clay  
 733 brick columns. The analysis of the results confirms evidencing that the predictions of the two models are on  
 734 average conservative, while the ACI formulation appears more accurate when referring to clay brick columns  
 735 confined with SRG systems.



736  
 737 **Fig. 26. Clay brick masonry columns: predicted/experimental comparison**

## 738 Conclusions

739 In this paper, a Round Robin experimental activity on the mechanical behavior of masonry columns confined  
 740 by using FRCM systems is reported and discussed. Eight Italian University laboratories were involved within  
 741 the framework of the ReLUIS-DPC 2019–2021 project (WP 14) funded by the *Italian Department of Civil*  
 742 *Protection*. Two reinforcing systems, namely GFRCM and SRG, were tested on two different kinds of  
 743 masonry, *Tuff* stone and clay brick, considering three reinforcing configurations (one-layer, two-layers and  
 744 three-layers of reinforcement). In total 64 specimens were tested. The obtained results were deeply analyzed  
 745 and compared in order to gain new insight on the confinement, mainly referring to the effect of reinforcement  
 746 configuration. The aim of this effort is valuable by considering that the available database is generally still  
 747 limited when referring to the confinement of existing masonry columns by means of FRCMs and mostly when  
 748 more than one layer is utilized for strengthening. The typical variability of masonry material, due to the  
 749 influence of scatters characterizing both the constituent materials (mortar and stones), the variability of  
 750 performances related to different manufacturing operators and the variability of utilized test setup from  
 751 different laboratories, even if starting from the same agreed scheme, caused in some cases significant  
 752 dispersion of experimental results. However, the carried out analysis can be considered very useful for the  
 753 scientific community as well as for standards assessment and validation.

754 On the basis of obtained results the following considerations can be drawn:

- 755 • As regards the masonry specimens confined by GFRCM the failure mode was almost similar in all  
 756 cases (*Tuff* stone and clay brick masonry), substantially characterized by the formation of one main  
 757 critical crack in correspondence of the edge at one corner of the member, where as expected a stress  
 758 concentration occurs, causing finally the mesh failure. SRG-confined *Tuff* masonry specimens showed  
 759 a different failure, characterized by the formation of different cracks (horizontal and vertical direction),  
 760 with final debonding of the reinforcement from the inner layer, mortar spalling or failure at the  
 761 overlapping zones.
- 762 • The effectiveness of the confinement by using GFRCM increased with the numbers of layers for both  
 763 kinds of tested masonry, even if following a different trend. In fact, in the case of *Tuff* masonry the  
 764 one-layer configuration provided for a negligible improvement in terms of compressive strength, while  
 765 the bearing capacity resulted almost 80% higher than that of reference specimens with three-layers of  
 766 GFRCM, and the trend increase appears almost linear passing from one to two layers of reinforcement.  
 767 As regards the clay-brick specimens an improvement of compressive strength was already registered

768 with one-layer reinforcement (34%) while increasing the number of composite layers the bearing  
769 capacity variation showed a reduced slope compared to the previous case, up to a bearing capacity  
770 increase of 74%, on average, for the case of three-layers configuration. This result remarks the  
771 influence of the mechanical properties of the composite in relation to those of the masonry; in fact, for  
772 a poor substrate the significant damage and, thus, the high expansion of the columns cannot be carried  
773 by the fibrous mesh of low density, typically used in FRCM systems. On the opposite, by increasing  
774 the reinforcement layers the confinement effectiveness increases as well attaining a relevant value. In  
775 the case of SRG systems confining clay bricks masonry the effectiveness of the confinement is higher  
776 than in the case of GFRM system even if similar values are attained, on average, for the two kinds of  
777 reinforcements in the case of three-layer configuration. On the other hand, when referring to *Tuff*  
778 masonry the greater benefit in case of SRG system is registered only with one-layer configuration. The  
779 increase in number of confining layers does not provide a proportional increase in effectiveness of  
780 confinement, probably due to the premature observed debonding phenomena. In addition, it can be  
781 observed that a higher deformability capacity is registered in all cases when the confinement is exerted  
782 by SRG systems, after the attainment of the maximum compressive stress. For all tested specimens  
783 the ultimate deformation registered on the composite is lower than that evaluated by tensile mechanical  
784 characterization; this result again confirms that in the case of FRCM/SRG systems a complex  
785 interaction between substrate, reinforcing textile and mortar matrix occurs; in particular, the  
786 mechanical properties of substrate/textile/mortar play a fundamental role, strongly affecting the proper  
787 activation of the passive confinement as well as the exploitation of its mechanical performances, the  
788 latter being influenced to a large extent also by the mortar properties.

- 789 • The obtained experimental results were used to understand the effectiveness of two available design-  
790 oriented formulas, reported in the Italian CNR (National Research Council) and ACI (American  
791 Concrete Institute) guidelines. Particular attention was devoted to check their effectiveness in case of  
792 multi-layers' reinforcement. The performed comparisons highlighted that the two design relationships  
793 provided for similar and accurate results when referring to the GFRCM system in one- and two- layer  
794 configurations, while the predictions appeared conservative when three- layers of GFRM are  
795 considered, irrespective of the type of masonry. Considering the SRG system, the results predicted by  
796 the two models are more scattered, mostly when the number of layers increases; in addition, the  
797 formulation proposed by CNR appears more accurate in case of *Tuff* masonry while the ACI  
798 predictions are closer to the experimental results in the case of clay brick masonry.

799 Further experimental programs are suggested in order to extend the available database to other kinds of  
800 reinforcement and masonry substrates, while considering a multi-ply configuration, in order to eventually  
801 address possible improvements of available design relationships.

## 804 **Conflict of interest**

805 The authors declare they to do not have any conflict of interest.

## 806 **Acknowledgments**

807  
808 The authors sincerely thank the Italian Department of Civil Protection for funding the present research within  
809 the RELUIS program 2019-2021 (WP14- Contributions for Standards Assessment regarding the use of  
810 Innovative Materials for Strengthening Existing Structures). A special acknowledgment is also addressed to  
811 FibreNet s.p.a. and Kerakoll s.p.a. for providing their materials and technical support.

812 **References**

- 813 [1] International Federation for Structural Concrete (*fib*). Externally applied FRP reinforcement for  
814 concrete structures. *fib Bulletin 90*. International Federation for Structural Concrete (*fib*); 2019.  
815 <https://doi.org/10.35789/fib.BULL.90>.
- 816 [2] Micelli, F., & Cascardi, A. (2020). Structural assessment and seismic analysis of a 14<sup>th</sup> century  
817 masonry tower. *Engineering Failure Analysis*, 107, 104198.
- 818 [3] Wu, Z., Wang X., Zhao X., & Mohammad, N. (2014). State-of-the-art review of FRP composites for  
819 major construction with high performance and longevity *Zhishen Int. J. Sustainable Materials and*  
820 *Structural Systems*, 1(3), 201-231.
- 821 [4] Ascione, F., Lamberti, M., Napoli, A., Razaqpur, G., & Realfonzo, R. (2017). An experimental  
822 investigation on the bond behavior of steel reinforced polymers on concrete substrate. *Composite*  
823 *Structures*, 181, 58-72.
- 824 [5] Teng, J.G., Jiang, T., Lam, L., & Luo, Y.Z. (2009). Refinement of a design-oriented stress–strain  
825 model for FRP-confined concrete. *Journal of Composites for Construction*; 13(4), 269–78.
- 826 [6] Ascione, F., Napoli, A., & Realfonzo, R. (2020). Interface bond between FRP systems and substrate:  
827 Analytical modeling. *Composite Structures*, Article number 112942 (in press).
- 828 [7] Babatunde, S.A. (2017). Review of strengthening techniques for masonry using fiber reinforced  
829 polymers. *Composite Structures*, 161, 246-255.
- 830 [8] Kreaikas, T.D., & Triantafillou, T.C. (2005). Masonry Confinement with Fiber-Reinforced Polymers.  
831 *Journal of Composites for Construction*, 9(2), 128–135.
- 832 [9] Faella, C., Martinelli, E., Camorani, G., Aiello, M.A., Micelli, F., & Nigro, E. (2011). Masonry  
833 columns confined by composite materials: Design formulae. *Composites: Part B*, 42, 705–716.
- 834 [10] Cascardi, A., Micelli, F., & Aiello, M. A. (2017). An Artificial Neural Networks model for the  
835 prediction of the compressive strength of FRP-confined concrete circular columns. *Engineering*  
836 *Structures*, 140, 199-208.
- 837 [11] Vaculik, J., Visintin, P., & Burton, N.G. (2018). Global database of FRP-to-masonry bond  
838 strength tests. *Data in Brief*, 20, 2065-2071.
- 839 [12] Cascardi, A., Leone, M., & Aiello, M. A. (2020). Transversal joining of multi-leaf masonry  
840 through different types of connector: Experimental and theoretical investigation. *Construction and*  
841 *Building Materials*, 265, 120733.
- 842 [13] Valluzzi, M. R. (2016). Challenges and perspectives for the protection of masonry structures  
843 in historic centers: the role of innovative materials and techniques. *RILEM Technical Letters*, 1, 45-  
844 49.
- 845 [14] ICOMOS/Isarsah Committee. (25). Recommendations for the analysis, conservation and  
846 structural restoration of architectural heritage. See [www.icomos.org](http://www.icomos.org)
- 847 [15] ACI Committee 549. Guide to Design and construction of externally bonded fabric-reinforced  
848 cementitious matrix (FRCM) systems for repair and strengthening concrete and masonry structures;  
849 ACI 549.4R-13. ACI, Farmington Hill, US; 2013.
- 850 [16] Bencardino, F., Carloni, C., Condello, A., Focacci, F., Napoli, A., & Realfonzo, R. (2018).  
851 Flexural behaviour of RC members strengthened with FRCM: State-of-the-art and predictive formulas.  
852 *Composites Part B: Engineering*, 148, 132-148.
- 853 [17] Papanicolaou, C. G., Triantafillou, T. C., Papathanasiou, M., & Karlos, K. (28). Textile  
854 reinforced mortar (TRM) versus FRP as strengthening material of URM walls: out-of-plane cyclic  
855 loading. *Materials and structures*, 41(1), 143-157.
- 856 [18] Ascione, F., Lamberti, M., Napoli, A., & Realfonzo, R. (2020). Experimental bond behavior  
857 of Steel Reinforced Grout systems for strengthening concrete elements. *Construction and Building*  
858 *Materials*, 232.
- 859 [19] De Felice, G., De Santis, S., Realfonzo, R., Napoli, A., Ascione F., Stievanin, E., Cescatti, E.,  
860 Valluzzi, M.R., Carloni, C., Santandrea, M., & Camata, G. (2018). State of the art of steel reinforced  
861 grout applications to strengthen masonry structures. American Concrete Institute, ACI Special  
862 Publication 2018, SP 326, 101.1-101.10.

- 863 [20] Campanini, D., Hadad, H. A., Carloni, C., Mazzotti, C., & Nanni, A. (2019). Mechanical  
864 Characterization of SRG Composites According to AC434. In *Key Engineering Materials* (Vol. 817,  
865 pp. 458-465). Trans Tech Publications Ltd.
- 866 [21] Cascardi, A., Micelli, F., & Aiello, M. A. (2016). Analytical model based on artificial neural  
867 network for masonry shear walls strengthened with FRM systems. *Composites Part B: Engineering*,  
868 95, 252-263.
- 869 [22] D'Antino, T., Carozzi, F. G., Colombi, P., & Poggi, C. (2018). Out-of-plane maximum  
870 resisting bending moment of masonry walls strengthened with FRCM composites. *Composite*  
871 *Structures*, 202, 881-896.
- 872 [23] Alecci, V., Focacci, F., Rovero, L., Stipo, G., & De Stefano, M. (2017). Intrados strengthening  
873 of brick masonry arches with different FRCM composites: Experimental and analytical investigations.  
874 *Composite Structures*, 176, 898-909.
- 875 [24] Sneed, L. H., Baietti, G., Fraioli, G., & Carloni, C. (2019). Compressive Behavior of Brick Masonry  
876 Columns Confined with Steel-Reinforced Grout Jackets. *Journal of Composites for Construction*,  
877 23(5), 04019037.
- 878 [25] Cascardi, A., Micelli, F., & Aiello, M. A. (2018). FRCM-confined masonry columns: experimental  
879 investigation on the effect of the inorganic matrix properties. *Construction and Building Materials*,  
880 186, 811-825.
- 881 [26] Ombres, L., & Verre, S. (2018). Masonry columns strengthened with Steel Fabric Reinforced  
882 Cementitious Matrix (S-FRCM) jackets: Experimental and numerical analysis. *Measurement*, 127,  
883 238-245.
- 884 [27] Di Ludovico, M., Cascardi, A., Balsamo, A., & Aiello, M. A. (2020). Uniaxial Experimental Tests on  
885 Full-Scale Limestone Masonry Columns Confined with Glass and Basalt FRCM Systems. *Journal of*  
886 *Composites for Construction*, 24(5), 040250.
- 887 [28] Ombres, L., & Verre, S. (2020). Analysis of the Behavior of FRCM Confined Clay Brick Masonry  
888 Columns. *Fibers*, 8(2), 11.
- 889 [29] Aiello, M.A.; Cascardi, A.; Ombres, L.; Verre, S. Confinement of Masonry Columns with the FRCM-  
890 System: Theoretical and Experimental Investigation. *Infrastructures* 2020, 5, 101.
- 891 [30] Micelli, F., Maddaloni, G., Longo, F., & Prota, A. Axial Stress–Strain Model for FRCM Confinement  
892 of Masonry Columns. *Journal of Composites for Construction*, 25(1), 040278.
- 893 [31] Cascardi, A., Dell'Anna, R., Micelli, F., Lionetto, F., Aiello, M. A., & Maffezzoli, A. (2019).  
894 Reversible techniques for FRP-confinement of masonry columns. *Construction and Building*  
895 *Materials*, 225, 415-428.
- 896 [32] National Research Council. Guide for the design and construction of externally bonded fibre reinforced  
897 inorganic matrix systems for strengthening existing structures. CNR-DT 215/2018. Rome, Italy, CNR,  
898 2020.
- 899 [33] Carozzi, F. G., Bellini, A., D'Antino, T., de Felice, G., Focacci, F., Hojdys, Ł., ... & Poggi, C. (2017).  
900 Experimental investigation of tensile and bond properties of Carbon-FRCM composites for  
901 strengthening masonry elements. *Composites Part B: Engineering*, 128, 1-119.
- 902 [34] De Santis, S., Ceroni, F., de Felice, G., Fagone, M., Ghiassi, B., Kwiecień, A., ... & Viskovic, A.  
903 (2017). Round Robin Test on tensile and bond behaviour of Steel Reinforced Grout systems.  
904 *Composites Part B: Engineering*, 127, 1-120.
- 905 [35] Leone, M., Aiello, M. A., Balsamo, A., Carozzi, F. G., Ceroni, F., Corradi, M., ... & Mazzotti, C.  
906 (2017). Glass fabric reinforced cementitious matrix: Tensile properties and bond performance on  
907 masonry substrate. *Composites Part B: Engineering*, 127, 196-214.
- 908 [36] Lignola, G. P., Caggegi, C., Ceroni, F., De Santis, S., Krajewski, P., Lourenço, P. B., ... & Zuccarino,  
909 L. (2017). Performance assessment of basalt FRCM for retrofit applications on masonry. *Composites*  
910 *Part B: Engineering*, 128, 1-18.
- 911 [37] Caggegi, C., Carozzi, F. G., De Santis, S., Fabbrocino, F., Focacci, F., Hojdys, Ł., ... & Zuccarino, L.  
912 (2017). Experimental analysis on tensile and bond properties of PBO and aramid fabric reinforced  
913 cementitious matrix for strengthening masonry structures. *Composites Part B: Engineering*, 127, 175-  
914 195.

- 915 [38] Santandrea, M., Focacci, F., Mazzotti, C., Ubertini, F., Carloni, C. (2020). Determination of the  
916 interfacial cohesive material law for SRG composites bonded to a masonry substrate. *Engineering*  
917 *Failure Analysis*, 2020, 111, 104322.
- 918 [39] Carozzi, F. G., Bellini, A., D'Antino, T., de Felice, G., Focacci, F., Hojdys, Ł., ... & Poggi, C. (2017).  
919 Experimental investigation of tensile and bond properties of Carbon-FRCM composites for  
920 strengthening masonry elements. *Composites Part B: Engineering*, 128, 1-119.
- 921 [40] International Code Council Evaluation Service (ICC-ES). Acceptance criteria for masonry and  
922 concrete strengthening using fabric-reinforced cementitious matrix (FRCM) and steel reinforced grout  
923 (SRG) composite systems. AC434. Whittier, CA: 2018.
- 924 [41] Incerti, A., Vasiliu, A., Ferracuti, B., & Mazzotti, C. (2015, December). Uni-Axial compressive tests  
925 on masonry columns confined by FRP and FRCM. In *Proc. of the 12th International Symposium on*  
926 *Fiber Reinforced Polymers for Reinforced Concrete Structures & The 5<sup>th</sup> Asia-Pacific Conference on*  
927 *Fiber Reinforced Polymers in Structures, Joint Conference, Nanjing, China, 14–16 December 2015*.
- 928 [42] Cascardi, A., Aiello, M. A., & Triantafillou, T. (2017). Analysis-oriented model for concrete and  
929 masonry confined with fiber reinforced mortar. *Materials and Structures*, 50(4), 202.
- 930 [43] Cascardi, A., Longo, F., Micelli, F., & Aiello, M. A. (2017). Compressive strength of confined column  
931 with Fiber Reinforced Mortar (FRM): New design-oriented-models. *Construction and Building*  
932 *Materials*, 156, 387-401.
- 933 [44] Balsamo, A., Cascardi, A., Di Ludovico, M., Aiello, M. A., & Morandini, G. (2018). Analytical study  
934 on the effectiveness of the FRCM-confinement of masonry columns. In *Construction Pathology,*  
935 *Rehabilitation. Technology and Heritage Management*.
- 936 [45] Ombres L. Confinement effectiveness in eccentrically loaded masonry columns strengthened by fiber  
937 reinforced cementitious matrix (FRCM) jackets. In *Vol. 624 of Key engineering materials*, 551–558.  
938 Zurich, Switzerland: Trans Tech Publications.
- 939 [46] Murgo, F.S., Mazzotti, C. (2019). Masonry columns strengthened with FRCM system: Numerical and  
940 experimental evaluation. *Construction and Building Materials*, 2019, 202, pp. 208-222.
- 941 [47] Kreaikas, T. D. (2019). Experimental study on carbon fiber textile reinforced mortar system as a  
942 means for confinement of masonry columns. *Construction and Building Materials*, 208, 723-733.
- 943 [48] Fossetti, M., & Minafò, G. (2017). Comparative experimental analysis on the compressive behaviour  
944 of masonry columns strengthened by FRP, BFRCM or steel wires. *Composites Part B: Engineering*,  
945 112, 112-124.
- 946 [49] EN 1015-11:27. Methods of test for mortar for masonry - Part 11: Determination of flexural and  
947 compressive strength of hardened mortar. CEN.
- 948 [50] EN 772-1:2011. Methods of test for masonry units - Part 1: Determination of compressive strength.  
949 CEN.
- 950 [51] UNI, *Metodi di prova per pietre naturali–Determinazione della resistenza a compressione uniassiale,*  
951 *27. [In Italian]*
- 952 [52] EN ISO 13934\_1:2013. Textiles — Tensile properties of fabrics — Part 1: Determination of maximum  
953 force and elongation at maximum force using the strip method.
- 954 [53] De Felice, G., Aiello, M. A., Caggegi, C., Ceroni, F., De Santis, S., Garbin, E., ... & Leone, M. (2018).  
955 Recommendation of RILEM Technical Committee 250-CSM: Test method for Textile Reinforced  
956 Mortar to substrate bond characterization. *Materials and Structures*, 51(4), 95.
- 957 [54] Ramaglia, G., Lignola, G. P., Fabbrocino, F., & Prota, A. (2019). Multi-parameters mechanical  
958 modeling to derive a confinement model for masonry columns. *Construction and Building Materials*,  
959 214, 303-317.
- 960 [55] Lignola, G.P., Angiuli, R., Prota, A., Aiello, M.A. (2014). FRP confinement of masonry:  
961 analytical modeling. *Materials and Structures*, 47 (12), 2101-2115.

962